Available online at www.sciencedirect.com
SCIENCE DIRECT®
Wave Motion 42 (2005) 238–260
WAVE MOTION
www.elsevier.com/locate/wavemoti

Time-reversal refocusing for point source in randomly layered media

Jean-Pierre Fouque[a], Josselin Garnier[b,*], André Nachbin[c], Knut Sølna[d]

[a] *Department of Mathematics, North Carolina State University, Raleigh, NC 27695-8205, USA*
[b] *Laboratoire de Probabilités et Modèles Aléatoires & Laboratoire Jacques-Louis Lions, Université Paris VII, 2 Place Jussieu, 75251 Paris Cedex 5, France*
[c] *Instituto de Matemática Pura e Aplicada, Est. D Castorina 110, Jardim Botânico, Rio de Janeiro, RJ 22460-320, Brazil*
[d] *Department of Mathematics, University of California, Irvine, CA 92697, USA*

Received 30 July 2004; received in revised form 22 February 2005; accepted 3 March 2005
Available online 8 April 2005

Abstract

This paper demonstrates the interest of a time-reversal method for the identification of source in a randomly layered medium. An active source located inside the medium emits a pulse that is recorded on a small time-reversal mirror. The wave is sent back into the medium, either numerically in a computer with the knowledge of the medium, or physically into the real medium. Our goal is to give a precise description of the refocusing of the pulse. We identify and analyze a regime where the pulse refocuses on a ring at the depth of the source and at a critical time. Our objective is to find the location of the source and we show that the time-reversal refocusing contains information which can be used to this effect and which cannot be obtained by a direct arrival-time analysis. The time-reversal technique gives a robust procedure to locate and characterize the source also in the case with ambient noise created by other sources located at the surface.

Keywords: Acoustic waves; Random media; Asymptotic theory; Time reversal

1. Introduction

In the regime of separation of scales a framework for analysis of acoustic waves propagating in randomly layered media has been set forth in [1]. The scale regime we consider corresponds to wavelengths that are large relative to the correlation length of the medium, but short relative to the depth of the source, moreover, we allow the

* Corresponding author. Tel.: +33 144278693; fax: +33 144277650.
E-mail addresses: fouque@math.ncsu.edu (J.-P. Fouque), garnier@math.jussieu.fr (J. Garnier), nachbin@impa.br (A. Nachbin), ksolna@math.uci.edu (K. Sølna)

0165-2125/$ – see front matter © 2005 Elsevier B.V. All rights reserved.
doi:10.1016/j.wavemoti.2005.03.001

random medium to have strong fluctuations. Here, we first generalize this framework to the case with a source inside of the medium. We then use this approach to implement time-reversal and analyze the refocusing properties of the wave field. Time-reversal refocusing for waves propagating in inhomogeneous media has been recently observed and studied experimentally in various contexts, e.g. ultrasound, underwater acoustics, see for instance the review [10]. Important potential applications have been proposed in various fields, for instance imaging [18,11] and communication [9]. A time-reversal mirror is, roughly speaking, a device which is capable of receiving a signal in time, keeping it in memory and sending it back into the medium in the reversed direction of time. The main effect is the refocusing of the scattered signal after time-reversal in a random medium. Surprisingly, the refocused pulse shape only depends on the statistical properties of the random medium, and not on the particular realization of the medium. The full mathematical understanding, meaning both modeling of the physical problem and derivation of the time-reversal effect, is a complex problem. The study of the one-dimensional case is now well understood [8,20,12] as well as the three-dimensional waves in the parabolic or paraxial regime [2,3,16].

Our analysis shows how time-reversal techniques can be useful for source estimation in the context of randomly layered media. We consider linear acoustic waves propagating in three spatial dimensions:

$$\rho\frac{\partial\vec{\mathbf{u}}}{\partial t}+\nabla p=\vec{\mathbf{F}},\qquad \frac{1}{K}\frac{\partial p}{\partial t}+\nabla\cdot\vec{\mathbf{u}}=0, \tag{1}$$

where p is the pressure, $\vec{\mathbf{u}}$ is the velocity, ρ is the density of the medium, and K the bulk modulus. The forcing term $\vec{\mathbf{F}}$ is due to the source. In order to simplify the analysis we consider the case with a constant density and a randomly fluctuating bulk modulus which is z-dependent only in the slab $(0, L)$. Note that we choose L so large that the termination of the slab does not affect the wave field at the surface $z = 0$ over the time period that we consider

$$\rho\equiv\rho_0,\qquad \frac{1}{K}=\begin{cases}\dfrac{1}{K_0}\left(1+\nu\left(\dfrac{z}{\varepsilon^2}\right)\right) & \text{if } -L<z<0,\\[2ex] \dfrac{1}{K_0} & \text{if } z>0 \text{ and } z<-L,\end{cases} \tag{2}$$

where ν is a zero-mean mixing process and ε^2 is a small dimensionless parameter that characterizes the ratio between the correlation length of the medium and the typical depth of the source. The average velocity is given by $c_0=\sqrt{K_0/\rho_0}$. A point source located at $(\mathbf{x}_s, z_s)$, $z_s \le 0$, generates a forcing term $\vec{\mathbf{F}}$ at time t_s given by:

$$\vec{\mathbf{F}}(t,\mathbf{x},z)=\vec{\mathbf{f}}\left(\frac{t-t_s}{\varepsilon}\right)\delta(\mathbf{x}-\mathbf{x}_s)\delta(z-z_s). \tag{3}$$

Note that the time duration of the source is short and scaled by ε which is large compared to the correlation length of the medium which is $\mathcal{O}(\varepsilon^2)$. In our time-reversal setup we locate a time-reversal mirror of spatial size $\mathcal{O}(\varepsilon)$ at the origin. Our setup is illustrated by the cartoon given in Fig. 1.

In Section 2 we derive an integral representation for the time reversed wave field which is obtained by taking a Fourier transform in the time and lateral space coordinates. This reduces the problem to a family of one- dimensional problems that can be analyzed by decomposing the wave field into right and left going waves. In Section 4 we consider the particular case where the source is at the surface ($z_s = 0$). We carry out a careful stationary phase

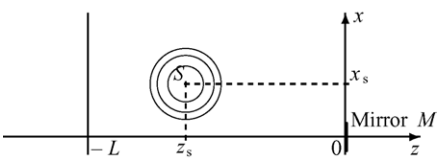

Fig. 1. Emission from a point source.

analysis combined with classic diffusion approximation results in the limit of small ε. This gives a limit with explicit formulas for the time reversed wave field which reveal a refocusing of the pulse at a critical time at the surface $z = 0$ and on a circle centered at the time-reversal mirror and passing through the source. If the time-reversal mirror only has point support the refocusing is uniform on the circle, while a small spatial extent mirror enables estimation of the angle to the source. In Section 5 we consider the important case with an internal source, also in this case we are able to carry out the asymptotic analysis that characterizes the limiting time reversed wave field. Even though the formulas are not explicit in this case we can still deduce the refocusing of the wave field and that it happens at a critical time, at the depth of the source and on a circle as in the previous case. In Section 6 we discuss a possible application to the problem of the source location and identification. In Section 7 we present numerical experiments which illustrate the results obtained in this paper.

2. The time reversed wave field

2.1. Emission from a point source

In the scaling that we consider the typical wavelength of the source is small $\mathcal{O}(\varepsilon)$ and we use the following specific Fourier transform and its inverse with respect to time and the transverse direction:

$$\hat{p}(\omega, \boldsymbol{\kappa}, z) = \int p(t, \mathbf{x}, z)\, \mathrm{e}^{\mathrm{i}(\omega/\varepsilon)(t-\boldsymbol{\kappa}\cdot\mathbf{x})}\, \mathrm{d}t\, \mathrm{d}\mathbf{x}, \qquad p(t, \mathbf{x}, z) = \frac{1}{(2\pi\varepsilon)^3} \int \hat{p}(\omega, \boldsymbol{\kappa}, z)\, \mathrm{e}^{-\mathrm{i}(\omega/\varepsilon)(t-\boldsymbol{\kappa}\cdot\mathbf{x})} \omega^2\, \mathrm{d}\omega\, \mathrm{d}\boldsymbol{\kappa},$$

where $\mathbf{x} = (x, y)$ stands for the transverse spatial variables. Taking the scaled Fourier transform gives that $\hat{\hat{\mathbf{u}}} = (\hat{\mathbf{v}}, \hat{u})^{\mathrm{T}}$ and $\hat{p}$ satisfy the system:

$$-\rho_0 \frac{\mathrm{i}\omega}{\varepsilon} \hat{\mathbf{v}} + \mathrm{i} \frac{\omega}{\varepsilon} \boldsymbol{\kappa} \hat{p} = \varepsilon \hat{\mathbf{f}}_{\mathbf{x}}(\omega)\, \mathrm{e}^{\mathrm{i}(\omega/\varepsilon)(t_{\mathrm{s}}-\boldsymbol{\kappa}\cdot\mathbf{x}_{\mathrm{s}})} \delta(z - z_{\mathrm{s}}), \tag{4}$$

$$-\rho_0 \frac{\mathrm{i}\omega}{\varepsilon} \hat{u} + \frac{\partial \hat{p}}{\partial z} = \varepsilon \hat{f}_z(\omega)\, \mathrm{e}^{\mathrm{i}(\omega/\varepsilon)(t_{\mathrm{s}}-\boldsymbol{\kappa}\cdot\mathbf{x}_{\mathrm{s}})} \delta(z - z_{\mathrm{s}}), \tag{5}$$

$$-\frac{1}{K(z)} \frac{\mathrm{i}\omega}{\varepsilon} \hat{p} + \mathrm{i} \frac{\omega}{\varepsilon} \boldsymbol{\kappa} \cdot \hat{\mathbf{v}} + \frac{\partial \hat{u}}{\partial z} = 0, \tag{6}$$

where $\hat{\hat{\mathbf{f}}} = (\hat{\mathbf{f}}_{\mathbf{x}}, \hat{f}_z)^{\mathrm{T}}$ is the ordinary unscaled Fourier transform of the source

$$\hat{\hat{\mathbf{f}}}(\omega) = \int \vec{\mathbf{f}}(t)\, \mathrm{e}^{\mathrm{i}\omega t}\, \mathrm{d}t, \qquad \vec{\mathbf{f}}(t) = \frac{1}{2\pi} \int \hat{\hat{\mathbf{f}}}(\omega)\, \mathrm{e}^{-\mathrm{i}\omega t}\, \mathrm{d}\omega.$$

We deduce that $(\hat{u}, \hat{p})$ satisfy the following closed system for $-L < z < z_{\mathrm{s}}$ and $z_{\mathrm{s}} < z < 0$

$$\frac{\partial \hat{u}}{\partial z} + \frac{\mathrm{i}\omega}{\varepsilon} \left(-\frac{1}{K(z)} + \frac{|\boldsymbol{\kappa}|^2}{\rho_0} \right) \hat{p} = 0, \tag{7}$$

$$\frac{\partial \hat{p}}{\partial z} - \frac{\mathrm{i}\omega}{\varepsilon} \rho_0 \hat{u} = 0 \tag{8}$$

with the jumps at $z = z_{\mathrm{s}}$ given by

$$[\hat{u}]_{z_{\mathrm{s}}} = \varepsilon \frac{\boldsymbol{\kappa} \cdot \hat{\mathbf{f}}_{\mathbf{x}}(\omega)}{\rho_0}\, \mathrm{e}^{\mathrm{i}(\omega/\varepsilon)(t_{\mathrm{s}}-\boldsymbol{\kappa}\cdot\mathbf{x}_{\mathrm{s}})}, \qquad [\hat{p}]_{z_{\mathrm{s}}} = \varepsilon \hat{f}_z(\omega)\, \mathrm{e}^{\mathrm{i}(\omega/\varepsilon)(t_{\mathrm{s}}-\boldsymbol{\kappa}\cdot\mathbf{x}_{\mathrm{s}})}. \tag{9}$$

We introduce the right and left propagating wave modes a and b which are defined by

$$\hat{p}(\omega,\boldsymbol{\kappa},z)=\frac{\sqrt{I_0(\kappa)}}{2}(a(\omega,\boldsymbol{\kappa},z)\,\mathrm{e}^{\mathrm{i}(\omega/\varepsilon)\zeta_0(\kappa)z}-b(\omega,\boldsymbol{\kappa},z)\,\mathrm{e}^{-\mathrm{i}(\omega/\varepsilon)\zeta_0(\kappa)z}), \tag{10}$$

$$\hat{u}(\omega,\boldsymbol{\kappa},z)=\frac{1}{2\sqrt{I_0(\kappa)}}(a(\omega,\boldsymbol{\kappa},z)\,\mathrm{e}^{\mathrm{i}(\omega/\varepsilon)\zeta_0(\kappa)z}+b(\omega,\boldsymbol{\kappa},z)\,\mathrm{e}^{-\mathrm{i}(\omega/\varepsilon)\zeta_0(\kappa)z}), \tag{11}$$

where $\kappa=|\boldsymbol{\kappa}|$, $\zeta_0^{-1}(\kappa)$ is the average longitudinal velocity, and $I_0(\kappa)$ is the acoustic impedance

$$\zeta_0(\kappa)=\frac{\sqrt{1-c_0^2\kappa^2}}{c_0},\qquad I_0(\kappa)=\frac{\rho_0}{\zeta_0(\kappa)}.$$

Here we only consider propagating modes and ignore evanescent modes meaning that $\kappa<c_0^{-1}$. The system for a and b can be written as

$$\frac{\partial}{\partial z}\begin{pmatrix}a\\b\end{pmatrix}(\omega,\kappa,z)=Q^{\varepsilon}(\omega,\kappa,z)\begin{pmatrix}a\\b\end{pmatrix}(\omega,\kappa,z), \tag{12}$$

$$Q^{\varepsilon}(\omega,\kappa,z)=\frac{\mathrm{i}\omega\zeta_0(\kappa)}{2\varepsilon(1-c_0^2\kappa^2)}\nu\left(\frac{z}{\varepsilon^2}\right)\begin{pmatrix}1 & -\mathrm{e}^{-2\mathrm{i}(\omega/\varepsilon)\zeta_0(\kappa)z}\\ \mathrm{e}^{2\mathrm{i}(\omega/\varepsilon)\zeta_0(\kappa)z} & -1\end{pmatrix}. \tag{13}$$

Using the definitions (10) and (11) of a and b and the expressions (9) for the jumps in $\hat{u}$ and $\hat{p}$ we deduce the jumps at $z=z_{\mathrm{s}}$ for the modes a and b

$$[a]_{z_{\mathrm{s}}}=\varepsilon\,\mathrm{e}^{\mathrm{i}(\omega/\varepsilon)(t_{\mathrm{s}}-\boldsymbol{\kappa}\cdot\mathbf{x}_{\mathrm{s}}-\zeta_0(\kappa)z_{\mathrm{s}})}S_a(\omega,\boldsymbol{\kappa}),\qquad [b]_{z_{\mathrm{s}}}=\varepsilon\,\mathrm{e}^{\mathrm{i}(\omega/\varepsilon)(t_{\mathrm{s}}-\boldsymbol{\kappa}\cdot\mathbf{x}_{\mathrm{s}}+\zeta_0(\kappa)z_{\mathrm{s}})}S_b(\omega,\boldsymbol{\kappa}) \tag{14}$$

with the source contributions given by

$$S_a(\omega,\boldsymbol{\kappa})=\frac{\sqrt{I_0(\kappa)}}{\rho_0}\boldsymbol{\kappa}\cdot\hat{\mathbf{f}}_{\mathbf{x}}(\omega)+\frac{1}{\sqrt{I_0(\kappa)}}\hat{f}_z(\omega),\qquad S_b(\omega,\boldsymbol{\kappa})=\frac{\sqrt{I_0(\kappa)}}{\rho_0}\boldsymbol{\kappa}\cdot\hat{\mathbf{f}}_{\mathbf{x}}(\omega)-\frac{1}{\sqrt{I_0(\kappa)}}\hat{f}_z(\omega).$$

The system for a and b is associated with boundary conditions at $z=0$ and $z=-L$ that are shown in Fig. 2. We assume that no energy is coming from $+\infty$ and $-\infty$, so that we get the radiation conditions $a(\omega,\boldsymbol{\kappa},-L)=0$ and $b(\omega,\boldsymbol{\kappa},0)=0$. The quantity of interest is the wave field at the surface which is completely characterized by $a(\omega,\boldsymbol{\kappa},0)$ since $b(\omega,\boldsymbol{\kappa},0)=0$. We transform this boundary value problem into an initial value problem by introducing the propagator $Y(\omega,\kappa,z_0,z)$, $-L\le z_0\le z\le 0$, which is a family of complex 2×2 matrices solutions of $\partial_z Y=Q^{\varepsilon}(\omega,\kappa,z)Y$, starting from $Y(\omega,\kappa,z_0,z=z_0)=\mathrm{Id}_{\mathbb{C}^2}$. By using the particular form of the matrix Q^{ε} in (13) one can show that if the column vector $(\alpha,\beta)^{\mathrm{T}}$ is solution of Eq. (12) with the initial conditions $\alpha(z_0,z=z_0)=1$, $\beta(z_0,z=z_0)=0$, then the column vector $(\bar{\beta},\bar{\alpha})^{\mathrm{T}}$ is another solution linearly independent of the first solution, so

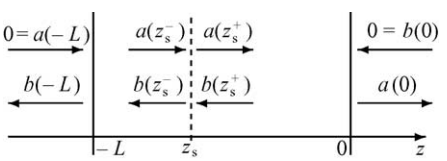

Fig. 2. Boundary conditions at $z=-L$ and $z=0$ corresponding to the emission from the point source located at depth z_{s}.

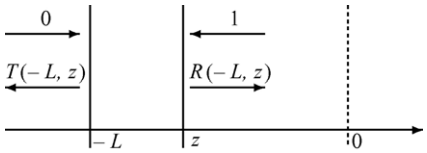

Fig. 3. Reflection and transmission coefficients.

that the propagator matrix Y can be written as:

$$Y(z_0, z) = \begin{pmatrix} \alpha & \bar{\beta} \\ \beta & \bar{\alpha} \end{pmatrix} (z_0, z).$$

The boundary conditions at $z = -L$ and $z = 0$ then imply

$$Y(-L, z_s) \begin{pmatrix} 0 \\ b(-L) \end{pmatrix} = \begin{pmatrix} a(z_s^-) \\ b(z_s^-) \end{pmatrix}, \qquad Y(z_s, 0) \begin{pmatrix} a(z_s^+) \\ b(z_s^+) \end{pmatrix} = \begin{pmatrix} a(0) \\ 0 \end{pmatrix}. \tag{15}$$

The system determined by ((14) and (15)) whose unknown are $b(-L)$ and $a(0)$ can be solved, and we get

$$a(\omega, \boldsymbol{\kappa}, 0) = \varepsilon\, \mathrm{e}^{\mathrm{i}(\omega/\varepsilon)(t_s - \boldsymbol{\kappa}\cdot\mathbf{x}_s)} [\mathrm{e}^{-\mathrm{i}(\omega/\varepsilon)\zeta_0(\kappa)z_s} T_g(\omega, \kappa, z_s) S_a(\omega, \boldsymbol{\kappa}) - \mathrm{e}^{\mathrm{i}(\omega/\varepsilon)\zeta_0(\kappa)z_s} R_g(\omega, \kappa, z_s) S_b(\omega, \boldsymbol{\kappa})], \tag{16}$$

$$R_g(\omega, \kappa, z) = \frac{(\bar{\beta}/\bar{\alpha})(\omega, \kappa, -L, z)}{\bar{\alpha}(\omega, \kappa, z, 0) + \beta(\omega, \kappa, z, 0)(\beta/\bar{\alpha})(\omega, \kappa, -L, z)}, \tag{17}$$

$$T_g(\omega, \kappa, z) = \frac{1}{\bar{\alpha}(\omega, \kappa, z, 0) + \beta(\omega, \kappa, z, 0)(\beta/\bar{\alpha})(\omega, \kappa, -L, z)}. \tag{18}$$

Observe the coefficients R_g and T_g are generalized versions of those used in [1] as we explain now. The transmission and reflection coefficients $T(\omega, \kappa - L, z)$ and $R(\omega, \kappa, -L, z)$ for a slab $[-L, z]$ (see Fig. 3) are given in terms of α and β as

$$R(\omega, \kappa, -L, z) = \frac{\bar{\beta}}{\bar{\alpha}}(\omega, \kappa, -L, z), \qquad T(\omega, \kappa, -L, z) = \frac{1}{\bar{\alpha}}(\omega, \kappa, -L, z).$$

We also introduce $\tilde{R}$ and $\tilde{T}$ defined as the reflection and transmission coefficients for the experiment corresponding to a right-going input wave incoming from the left (see Fig. 4). They are given in terms of α and β by

$$\tilde{R}(\omega, \kappa, z, 0) = -\frac{\beta}{\bar{\alpha}}(\omega, \kappa, z, 0), \qquad \tilde{T}(\omega, \kappa, z, 0) = \frac{1}{\bar{\alpha}}(\omega, \kappa, z, 0).$$

We can express the coefficients R_g and T_g in terms of the usual reflection and transmission coefficients R and T for which the asymptotic analysis of the moments has been carried out in [1] and will be used in subsequent sections.

$$R_g(\omega, \kappa, z) = \frac{\tilde{T}(\omega, \kappa, z, 0) R(\omega, \kappa, -L, z)}{1 - \tilde{R}(\omega, \kappa, z, 0) R(\omega, \kappa, -L, z)}, \tag{19}$$

$$T_g(\omega, \kappa, z) = \frac{\tilde{T}(\omega, \kappa, z, 0)}{1 - \tilde{R}(\omega, \kappa, z, 0) R(\omega, \kappa, -L, z)}. \tag{20}$$

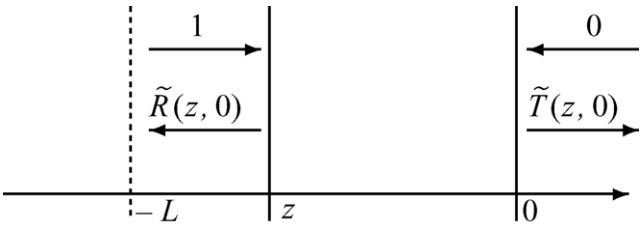

Fig. 4. Adjoint reflection and transmission coefficients.

We denote the wave at the surface $z = 0$ by $(\mathbf{u}_s, p_s)$. We have in particular

$$u_s(t,\mathbf{x}) = \frac{1}{(2\pi\varepsilon)^3}\int \frac{1}{2\sqrt{I_0(\kappa)}} a(\omega,\boldsymbol{\kappa},0)\mathrm{e}^{-\mathrm{i}(\omega/\varepsilon)(t-\boldsymbol{\kappa}\cdot\mathbf{x})}\omega^2\,\mathrm{d}\omega\,\mathrm{d}\boldsymbol{\kappa}. \tag{21}$$

These signals comprise a coherent front wave of duration $\mathcal{O}(\varepsilon)$ corresponding to the duration of the source, moreover, a long noisy coda part that is caused by the multiple scattering by the layers. These coda waves are a part of, and play a crucial role in, the time-reversal procedure that we describe next.

2.2. Recording, time-reversal and reemission

The first step of the time-reversal procedure consists in recording the velocity signal at $z = 0$ at the mirror $M = \{(\mathbf{x}, z), \mathbf{x} \in D^\varepsilon, z = 0\}$ during some time interval centered at $t = 0$. $D^\varepsilon \subset \mathbb{R}^2$ is the shape of the mirror whose center is located at point $\mathbf{0}$. It turns out that as $\varepsilon \to 0$ the interesting asymptotic regime arises when we record the signal during a large time interval whose duration is of order 1 and is denoted by t_1 with $t_1 > 0$. We consider here the practical situation where the mirror is not very large, but of a size of the order of a few wavelengths (i.e. of order ε).

In the second step of the time-reversal procedure a piece of the recorded signal is clipped using a cut-off function $s \mapsto G_1(s)$, where the support of G_1 is included in $[-t_1/2, t_1/2]$. We denote the recorded part of the wave by $\vec{\mathbf{u}}_{\mathrm{rec}}$ so that

$$\vec{\mathbf{u}}_{\mathrm{rec}}(t,\mathbf{x}) = \vec{\mathbf{u}}_s(t,\mathbf{x})G_1(t)G_2\left(\frac{\mathbf{x}}{\varepsilon}\right),$$

where G_2 is the spatial cut-off function introduced by the mirror of typical size ε with $G_2(\mathbf{x}) = \mathbf{1}_D(\mathbf{x})$ and D is the normalized shape of the mirror. We then time reverse this piece of signal and send it back into the same medium as illustrated in Fig. 5. This means that we address a new problem defined by the acoustic equations (1) with the source term

$$\vec{\mathbf{F}}_{\mathrm{TR}}(t,\mathbf{x},z) = \vec{\mathbf{f}}_{\mathrm{TR}}(t,\mathbf{x})\delta(z), \qquad \vec{\mathbf{f}}_{\mathrm{TR}}(t,\mathbf{x}) = \rho_0 c_0 \vec{\mathbf{u}}_{\mathrm{rec}}(-t,\mathbf{x}),$$

where TR stands for "time reversal" and the factor $\rho_0 c_0$ has been added to restore the physical dimension of the expression. Note that by linearity of the problem this factor plays no role in the analysis. In terms of right and left-going wave modes, the system consists of the linear system (12) for $-L \le z < 0$, with the boundary conditions $b_{\mathrm{TR}}(\omega,\boldsymbol{\kappa},0^+) = 0$, $a_{\mathrm{TR}}(\omega,\boldsymbol{\kappa},-L) = 0$, see Fig. 6, and the jump condition at $z = 0$ imposed by the source $\vec{\mathbf{F}}_{\mathrm{TR}}$

$$[b_{\mathrm{TR}}]_0 = \frac{\sqrt{I_0(\kappa)}}{\rho_0}\boldsymbol{\kappa}\cdot\hat{\mathbf{f}}_{\mathrm{TR},\mathbf{x}}(\omega,\boldsymbol{\kappa}) - \frac{1}{\sqrt{I_0(\kappa)}}\hat{f}_{\mathrm{TR},z}(\omega,\boldsymbol{\kappa}).$$

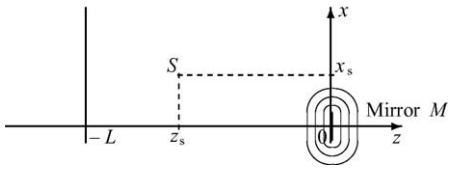

Fig. 5. Emission from the mirror.

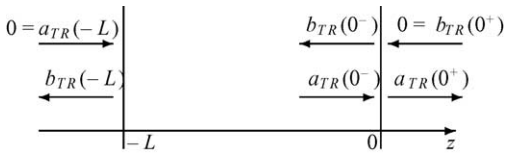

Fig. 6. Boundary conditions at $z = -L$ and $z = 0$ corresponding to the emission from the mirror located at $z = 0$.

Using $b_{\mathrm{TR}}(0^-) = -[b_{\mathrm{TR}}]_0$ and substituting the integral representation of the recorded velocity field into $\vec{\mathbf{F}}_{\mathrm{TR}}$, we deduce the boundary condition at $z = 0^-$

$$b_{\mathrm{TR}}(\omega, \boldsymbol{\kappa}, 0^-) = \frac{1}{(2\pi)^3 \varepsilon} \int \frac{H_0(\boldsymbol{\kappa}, \boldsymbol{\kappa}')}{2} \bar{a}(\omega', \boldsymbol{\kappa}', 0) \bar{\hat{G}}_1 \left(\frac{\omega - \omega'}{\varepsilon} \right) \hat{G}_2(\omega \boldsymbol{\kappa} + \omega' \boldsymbol{\kappa}') \omega'^2 \, \mathrm{d}\omega' \, \mathrm{d}\boldsymbol{\kappa}', \tag{22}$$

where

$$H_0(\boldsymbol{\kappa}, \boldsymbol{\kappa}') = \frac{\rho_0 c_0}{\sqrt{I_0(\kappa) I_0(\kappa')}} - \frac{\rho_0 c_0 \sqrt{I_0(\kappa) I_0(\kappa')}}{\rho_0^2} \boldsymbol{\kappa} \cdot \boldsymbol{\kappa}',$$

the quantity $a(\omega, \boldsymbol{\kappa}, 0)$ is given by (16), and the Fourier transformed window functions are defined by

$$\hat{G}_1(\omega) = \int G_1(t) \, \mathrm{e}^{\mathrm{i}\omega t} \, \mathrm{d}t, \qquad \hat{G}_2(\mathbf{k}) = \int G_2(\mathbf{x}) \, \mathrm{e}^{-\mathrm{i}\mathbf{k}\cdot\mathbf{x}} \, \mathrm{d}\mathbf{x}.$$

The configuration at hand can thus be reduced to the system (12) for $-L \le z < 0$ with the boundary conditions (22) at $z = 0$ and $a_{\mathrm{TR}}(\omega, \boldsymbol{\kappa}, -L) = 0$ at $z = -L$. The Fourier transformed pressure and velocity are now given by (10) and (11) where a and b are replaced by a_{TR} and b_{TR}.

2.3. The time reversed wave field

The new incoming signal propagates into the same medium and produces the time reversed wave field. Here we derive an exact integral representation for this wave field which will be exploited to analyze the refocusing properties of the time reversed field in the following sections. Using once again the propagator we get that the wave for $-L \le z \le 0$ is given by

$$u_{\mathrm{TR}}(t, \mathbf{x}, z) = \frac{1}{(2\pi\varepsilon)^3} \int \frac{1}{2\sqrt{I_0(\kappa)}} b_{\mathrm{TR}}(\omega, \boldsymbol{\kappa}, 0^-) [R_{\mathrm{g}}(\omega, \kappa, z) \, \mathrm{e}^{\mathrm{i}(\omega/\varepsilon)\zeta_0(\kappa)z} + T_{\mathrm{g}}(\omega, \kappa, z) \, \mathrm{e}^{-\mathrm{i}(\omega/\varepsilon)\zeta_0(\kappa)z}] \, \mathrm{e}^{-\mathrm{i}(\omega/\varepsilon)(t - \boldsymbol{\kappa}\cdot\mathbf{x})} \omega^2 \, \mathrm{d}\omega \, \mathrm{d}\boldsymbol{\kappa},$$

and similar expressions hold for $p_{\mathrm{TR}}(t,\mathbf{x},z)$ and $\mathbf{v}_{\mathrm{TR}}(t,\mathbf{x},z)$. Substituting the expression of $b_{\mathrm{TR}}(\omega,\boldsymbol{\kappa},0^-)$ into this equation yields the following representation of the longitudinal velocity

$$u_{\mathrm{TR}}(t,\mathbf{x},z)=\frac{1}{(2\pi)^6\varepsilon^3}\int\int\frac{H_0(\boldsymbol{\kappa}_1,\boldsymbol{\kappa}_2)}{4\sqrt{I_0(\kappa_1)}}\bar{\hat{G}}_1\left(\frac{\omega_1-\omega_2}{\varepsilon}\right)\hat{G}_2(\omega_1\boldsymbol{\kappa}_1+\omega_2\boldsymbol{\kappa}_2)\,\mathrm{e}^{\mathrm{i}(-(\omega_2 t_{\mathrm{s}}+\omega_1 t)+(\omega_2\boldsymbol{\kappa}_2\cdot\mathbf{x}_{\mathrm{s}}+\omega_1\boldsymbol{\kappa}_1\cdot\mathbf{x}))/\varepsilon}$$
$$\times\left[\sum_{j=1}^{4}P_j\right]\omega_1^2\omega_2^2\,\mathrm{d}\omega_1\,\mathrm{d}\boldsymbol{\kappa}_1\,\mathrm{d}\omega_2\,\mathrm{d}\boldsymbol{\kappa}_2, \tag{23}$$

where we define the P_j's by

$$P_1=-\mathrm{e}^{\mathrm{i}(-\omega_2\zeta_0(\kappa_2)z_{\mathrm{s}}+\omega_1\zeta_0(\kappa_1)z)/\varepsilon}\bar{R}_{\mathrm{g}}(\omega_2,\kappa_2,z_{\mathrm{s}})R_{\mathrm{g}}(\omega_1,\kappa_1,z)\bar{S}_b(\omega_2,\boldsymbol{\kappa}_2),$$
$$P_2=\mathrm{e}^{\mathrm{i}(\omega_2\zeta_0(\kappa_2)z_{\mathrm{s}}+\omega_1\zeta_0(\kappa_1)z)/\varepsilon}\bar{T}_{\mathrm{g}}(\omega_2,\kappa_2,z_{\mathrm{s}})R_{\mathrm{g}}(\omega_1,\kappa_1,z)\bar{S}_a(\omega_2,\boldsymbol{\kappa}_2),$$
$$P_3=\mathrm{e}^{\mathrm{i}(\omega_2\zeta_0(\kappa_2)z_{\mathrm{s}}-\omega_1\zeta_0(\kappa_1)z)/\varepsilon}\bar{T}_{\mathrm{g}}(\omega_2,\kappa_2,z_{\mathrm{s}})T_{\mathrm{g}}(\omega_1,\kappa_1,z)\bar{S}_a(\omega_2,\boldsymbol{\kappa}_2),$$
$$P_4=-\mathrm{e}^{\mathrm{i}(-\omega_2\zeta_0(\kappa_2)z_{\mathrm{s}}-\omega_1\zeta_0(\kappa_1)z)/\varepsilon}\bar{R}_{\mathrm{g}}(\omega_2,\kappa_2,z_{\mathrm{s}})T_{\mathrm{g}}(\omega_1,\kappa_1,z)\bar{S}_b(\omega_2,\boldsymbol{\kappa}_2).$$

In the following sections we study the asymptotic behavior of the time reversed wave field u_{TR} in the limit $\varepsilon\to 0$. We first address the case of a homogeneous medium in Section 3.

As we shall study the problem of the source location and contrast the homogeneous and random configurations. In the case of a random medium the analysis is carried out in the particular case where the source is located on the surface ($z_{\mathrm{s}}=0$) in Section 4, and in the general case where the source is inside of the medium ($z_{\mathrm{s}}<0$) in Section 5.

3. Homogeneous medium

We first examine the deterministic case with $\nu\equiv 0$ which corresponds to a homogeneous medium. The time reversed wave field is then described by (23) with $R_{\mathrm{g}}=0$ and $T_{\mathrm{g}}=1$. In this case only the P_3 term in u_{TR} corresponding to direct transmission paths contributes. Using the notation $\vec{\mathbf{r}}=(\mathbf{x},z)$, for small ε the leading order part of the three-dimensional velocity field is

$$\vec{\mathbf{u}}_{\mathrm{s}}(t,\vec{\mathbf{r}})=\frac{\vec{\mathbf{r}}-\vec{\mathbf{r}}_{\mathrm{s}}}{4\pi\rho_0 c_0^2\varepsilon|\vec{\mathbf{r}}-\vec{\mathbf{r}}_{\mathrm{s}}|^3}(\vec{\mathbf{r}}-\vec{\mathbf{r}}_{\mathrm{s}})\cdot\vec{\mathbf{f}}'\left(\frac{t-t_{\mathrm{s}}-(|\vec{\mathbf{r}}-\vec{\mathbf{r}}_{\mathrm{s}}|/c_0)}{\varepsilon}\right). \tag{24}$$

These expressions are derived from (21) and the Weyl representation of a spherical wave [16, Section 3.2.4], but they could also be derived directly from the fact that a point source emits a spherical wave that propagates at velocity c_0 in a homogeneous medium.

Let us next consider the time-reversed field. For the sake of simplicity we address the case with a spatial mirror that has point support so that $\hat{G}_2(\mathbf{k})$ is a constant denoted by $\hat{g}_2$. In this case we find

$$\vec{\mathbf{u}}_{\mathrm{TR}}(t,\mathbf{r})=-\frac{\hat{g}_2}{(4\pi)^2\rho_0 c_0^3}\frac{(\vec{\mathbf{r}}\cdot\vec{\mathbf{r}}_{\mathrm{s}})\vec{\mathbf{r}}}{|\vec{\mathbf{r}}_{\mathrm{s}}|^3|\vec{\mathbf{r}}|^3}G_1\left(\frac{|\vec{\mathbf{r}}|}{c_0}-t\right)\vec{\mathbf{r}}_{\mathrm{s}}\cdot\vec{\mathbf{f}}''\left(\frac{(|\vec{\mathbf{r}}|-|\vec{\mathbf{r}}_{\mathrm{s}}|)/c_0-t-t_{\mathrm{s}}}{\varepsilon}\right). \tag{25}$$

This is a spherical wave emerging from the mirror. Its support at a given time t is an ε neighborhood of the sphere with center at $\mathbf{0}$ and radius $|\vec{\mathbf{r}}_{\mathrm{s}}|+c_0(t+t_{\mathrm{s}})$. Observe that $\vec{\mathbf{u}}_{\mathrm{TR}}$ is of order 1 only if the signal originating from the original source has been recorded, meaning that $|\vec{\mathbf{r}}_{\mathrm{s}}|+c_0 t_{\mathrm{s}}$ lies in the support of G_1. Finally, note that the longitudinal velocity u_{TR} is vanishing at the surface $z=0$.

4. The random case with an exterior point source

In this section we assume that the source is located on the surface ($\mathbf{x}_s, z_s = 0$). We also observe the time-reversed wave at the surface ($\mathbf{x}, z = 0$). Under such conditions the generalized transmission and reflection coefficients T_g and R_g are evaluated at $z = 0$ and from their definitions, (19) and (20), it follows that the transmission coefficient T_g is equal to 1, and the reflection coefficient R_g corresponds to the reflections from the whole random medium between $-L$ and the surface, that is to say $R(-L, 0)$. The deterministic P_3 term of u_{TR} is associated with a product of transmission coefficients, it corresponds to recording and reemission of the directly transmitted wave field from the source to the mirror and then observation of the wave field that is directly transmitted back to the source point. As shown in Section 3 this component of u_{TR} is vanishing at the surface. The P_2 and P_4 terms are associated with one transmission and one reflection coefficient, they correspond respectively to (i) the wave that is directly transmitted to the mirror, then time reversed, re-emitted into the random medium and subsequently scattered back from the random medium and onto the recorder at the source point, (ii) the wave component that is reflected from the random medium onto the mirror then time reversed and transmitted directly back to the recorder at the source point. The P_1 term, the one defined in terms of a product of reflection coefficients, corresponds to the wave which has been scattered back twice by the random medium. From the point of view of refocusing of time reversed waves in a random medium this last term turns out to be the most interesting one.

We consider the P_1 term of the expression (23) of the longitudinal velocity. Due to the fact that the reflection coefficient only depends on the moduli of the slowness vectors, we use polar coordinates (μ_1, θ_1) and (μ_2, θ_2) for $\boldsymbol{\kappa}_1 = \mu_1 \mathbf{e}_{\theta_1}$ and $\boldsymbol{\kappa}_2 = \mu_2 \mathbf{e}_{\theta_2}$. We also represent the observation point $\mathbf{x}$ and the source position $\mathbf{x}_s$ by $r_0 \mathbf{e}_{\theta_0}$ and $r_s \mathbf{e}_{\theta_s}$, respectively, where we denote by $\mathbf{e}_\theta$ the unit column vector $(\cos(\theta), \sin(\theta))^T$. We show in Appendix A.2 that the reflection coefficients at two frequencies and slowness vectors are correlated only if the frequencies and the moduli of the slowness vectors are close to each other at order ε. Motivated by this remark we perform the change of variables $\omega_2 = \omega + \varepsilon h/2$, $\omega_1 = \omega - \varepsilon h/2$, $\mu_2 = \mu + \varepsilon\lambda/2$, and $\mu_1 = \mu - \varepsilon\lambda/2$. The representation of the P_1 term of the longitudinal velocity field becomes

$$
\begin{aligned}
u_{TR}^{(1)}(t, \mathbf{x} = r_0 \mathbf{e}_{\theta_0}, 0) = -\frac{1}{(2\pi)^6 \varepsilon} \int\int \frac{H_0(\mu \mathbf{e}_\theta, \mu \mathbf{e}_{\theta'})}{4\sqrt{I_0(\mu)}} \bar{\hat{G}}_1(-h) \hat{G}_2(\omega\mu(\mathbf{e}_\theta + \mathbf{e}_{\theta'})) \bar{S}_b(\omega, \mu \mathbf{e}_{\theta'})\, \mathrm{e}^{\mathrm{i}\phi(\omega,\mu,\theta,\theta')/\varepsilon} \\
\times \mathrm{e}^{(\mathrm{i}/2)(h(t-t_s)+(\lambda\omega+h\mu)[r_s\cos(\theta_s-\theta')-r_0\cos(\theta_0-\theta)])}\, \bar{R}\left(\omega + \frac{\varepsilon h}{2}, \mu + \frac{\varepsilon\lambda}{2}, -L, 0\right) \\
\times R\left(\omega - \frac{\varepsilon h}{2}, \mu - \frac{\varepsilon\lambda}{2}, -L, 0\right) \omega^4 \mu^2\, \mathrm{d}\lambda\, \mathrm{d}h\, \mathrm{d}\omega\, \mathrm{d}\mu\, \mathrm{d}\theta\, \mathrm{d}\theta',
\end{aligned}
$$

where the rapid phase is

$$
\phi(\omega, \mu, \theta, \theta') = \omega[-(t_s + t) + \mu(r_s \cos(\theta_s - \theta') + r_0 \cos(\theta_0 - \theta))],
$$

and we have neglected lower order terms (with respect to ε) by assuming that H_0 and $\hat{G}_2$ are smooth functions. As $\varepsilon \to 0$ the asymptotic behavior of this integral is governed by its fast phase and by the product of the two reflection coefficients which contains the effect of randomness. We first apply the *stationary phase method* and we will deal with the random part of the integral in a second step. The variables of the rapid phase are ω, μ, θ, and θ'. We find that there exist stationary points only if $t + t_s = 0$ and $r_0 = r_s$. Then there exist two maps of stationary points corresponding to

$$
\text{(I)} \quad \theta' = \theta_s \text{ and } \theta = \theta_0 + \pi, \qquad \text{(II)} \quad \theta' = \theta_s + \pi \text{ and } \theta = \theta_0.
$$

We then consider an observation time t close to $-t_s$. Similarly we consider an observation point $\mathbf{x}$ whose modulus is close to r_s. This is realized by the following parameterization $t = -t_s + \varepsilon\mathcal{T}$, $\mathbf{x} = r_s\mathbf{e}_{\theta_0} + \varepsilon\mathcal{R}\mathbf{e}_\phi$. We deduce that the P_1 term of the longitudinal velocity field consists of the sum of two terms corresponding to the contributions of the two maps of stationary points and we write

$$
\begin{aligned}
u_{\mathrm{TR}}^{(1)}(t,\mathbf{x},0) &= u_{\mathrm{TR}}^{(1,\mathrm{I})}(t,\mathbf{x},0) + u_{\mathrm{TR}}^{(1,\mathrm{II})}(t,\mathbf{x},0),\\
u_{\mathrm{TR}}^{(1,\mathrm{I})}(t,\mathbf{x},0) &= -\frac{1}{2^7\pi^5 r_s}\int\int \frac{H_0(-\mu\mathbf{e}_{\theta_0},\mu\mathbf{e}_{\theta_s})}{\sqrt{I_0(\mu)}}\bar{\hat{G}}_1(-h)\hat{G}_2(\omega\mu(\mathbf{e}_{\theta_s}-\mathbf{e}_{\theta_0}))\bar{S}_b(\omega,\mu\mathbf{e}_{\theta_s})\\
&\quad\times \mathrm{e}^{\mathrm{i}(-\omega\mathcal{T}-ht_s+r_s(\lambda\omega+h\mu)-\omega\mu\mathcal{R}\cos(\theta_0-\phi))}\,\bar{R}\left(\omega+\frac{\varepsilon h}{2},\mu+\frac{\varepsilon\lambda}{2},-L,0\right)\\
&\quad\times R\left(\omega-\frac{\varepsilon h}{2},\mu-\frac{\varepsilon\lambda}{2},-L,0\right)\omega^3\mu\,\mathrm{d}\lambda\,\mathrm{d}h\,\mathrm{d}\omega\,\mathrm{d}\mu,\\
u_{\mathrm{TR}}^{(1,\mathrm{II})}(t,\mathbf{x},0) &= -\frac{1}{2^7\pi^5 r_s}\int\int \frac{H_0(\mu\mathbf{e}_{\theta_0},-\mu\mathbf{e}_{\theta_s})}{\sqrt{I_0(\mu)}}\bar{\hat{G}}_1(-h)\hat{G}_2(\omega\mu(\mathbf{e}_{\theta_0}-\mathbf{e}_{\theta_s}))\bar{S}_b(\omega,-\mu\mathbf{e}_{\theta_s})\\
&\quad\times \mathrm{e}^{\mathrm{i}(-\omega\mathcal{T}-ht_s-r_s(\lambda\omega+h\mu)+\omega\mu\mathcal{R}\cos(\theta_0-\phi))}\,\bar{R}\left(\omega+\frac{\varepsilon h}{2},\mu+\frac{\varepsilon\lambda}{2},-L,0\right)\\
&\quad\times R\left(\omega-\frac{\varepsilon h}{2},\mu-\frac{\varepsilon\lambda}{2},-L,0\right)\omega^3\mu\,\mathrm{d}\lambda\,\mathrm{d}h\,\mathrm{d}\omega\,\mathrm{d}\mu.
\end{aligned}
$$

The effect of the randomness is contained in the product of the reflection coefficients. The asymptotic analysis of the autocorrelation function summarized in Appendix A.2 can then be exploited to deduce the refocusing properties of the pulse and its self-averaging property. The deterministic component of the time reversed wave given by the P_3 term is a spherical wave that is explicitly known and described in Section 3. Using the decorrelation property (A.5) explained in Appendix A.2, one can deduce that the contributions of the P_2 and P_4 terms vanish in the limit $\varepsilon \to 0$, so it remains only to study the P_1 term. Our stationary phase analysis presented here above shows that, for fixed observation time t and position $\mathbf{x}$, with $t + t_s \neq 0$ or $|\mathbf{x}| - r_s \neq 0$, there are no stationary points and $u_{\mathrm{TR}}(t,\mathbf{x},0)$ goes to *0* as $\varepsilon \to 0$. On the other hand, if $t = -t_s$ and $|\mathbf{x}| = r_s$, then there are maps of stationary points so a refocused pulse with amplitude of order 1 will be observed in an ε-neighborhood of $(-t_s, r_s)$. These results are precisely stated in the following theorem which gives the convergence of the refocused pulse to a deterministic shape concentrated at $-t_s$ in time and on a ring with radius r_s in space.

Theorem 4.1.

(a) *For any $\mathcal{T}_0 > 0$, $\mathcal{R}_0 > 0$, $\delta > 0$, and $(t_0, r_0) \neq (-t_s, r_s)$, we have*

$$
\mathbb{P}\left(\sup_{|t-t_0|\le\varepsilon\mathcal{T}_0,\,||\mathbf{x}|-r_0|\le\varepsilon\mathcal{R}_0}|u_{\mathrm{TR}}(t,\mathbf{x})| > \delta\right)\xrightarrow{\varepsilon\to 0} 0.
$$

(b) *For any $\mathcal{T}_0 > 0$, $\mathcal{R}_0 > 0$, $\delta > 0$, we have*

$$
\mathbb{P}\left(\sup_{|t+t_s|\le\varepsilon\mathcal{T}_0,\,||\mathbf{x}|-r_s|\le\varepsilon\mathcal{R}_0}\left|u_{\mathrm{TR}}(t,\mathbf{x}) - U_{\mathrm{TR}}\left(\frac{t+t_s}{\varepsilon},\frac{|\mathbf{x}|-r_s}{\varepsilon}\right)\right| > \delta\right)\xrightarrow{\varepsilon\to 0} 0,
$$

where U_{TR} is the deterministic pulse shape

$$U_{\mathrm{TR}}(\mathcal{T},\mathcal{R}) = \frac{1}{(2\pi)^3}\int \hat{K}(\omega,\mu)\left[\frac{\mu}{2\rho_0}\mathbf{e}_{\theta_s}\cdot\bar{\hat{\mathbf{f}}}_{\mathbf{x}}(\omega) + \frac{1}{2I_0(\mu)}\bar{\hat{f}}_z(\omega)\right] \mathrm{e}^{\mathrm{i}\omega(\mu\mathcal{R}-\mathcal{T})}\omega^2\,\mathrm{d}\omega\,\mathrm{d}\mu,$$

with the kernel $\hat{K}$ given by

$$\hat{K}(\omega,\mu) = \hat{G}_2(\omega\mu(\mathbf{e}_{\theta_0}-\mathbf{e}_{\theta_s}))G_1\left(t_s+\frac{r_s}{c_0^2\mu}\right)Q_1\left(\frac{\zeta_0(\mu)}{2\mu}r_s\right)\frac{\zeta_0(\mu)}{2}\frac{H_0(\mu\mathbf{e}_{\theta_0},-\mu\mathbf{e}_{\theta_s})}{2r_s}.$$

All the random effects on the refocused pulse are contained in Q_1 given by Eq. (A.3). Q_1 characterizes the limit of the autocorrelation function of the reflection coefficient. Note that Q_1 depends only on the integrated covariance of the fluctuations of the medium $\gamma_0 = \int_0^\infty \mathbb{E}[\nu(0)\nu(z)]\,\mathrm{d}z$. An explicit expression for H_0 is

$$H_0(\mu\mathbf{e}_{\theta_0},-\mu\mathbf{e}_{\theta_s}) = \zeta_0(\mu)c_0 + \frac{c_0\mu^2}{\zeta_0(\mu)}\mathbf{e}_{\theta_0}\cdot\mathbf{e}_{\theta_s}. \tag{26}$$

Similarly, the asymptotic deterministic shapes of the refocused transverse velocity and pressure fields consist of the sums of the deterministic components exhibited in Section 3 and of new components of the same form as U_{TR} resulting from the refocusing of the incoherent waves recorded at the mirror. The proof of the theorem is a generalization of the arguments given in [8] and goes along the following main steps.

- We first consider the expected value of $u_{\mathrm{TR}}^{(1)}$. Using a combination of stationary phase and the asymptotic behavior (A.4) of the autocorrelation function of the reflection coefficient we find that this expectation converges to the limiting value given in Theorem 4.1.
- We then consider the variance of $u_{\mathrm{TR}}^{(1)}$. We write the second moment as a multiple integral involving the product of four reflection coefficients at four different frequencies as in (A.5). Using the decorrelation property of the reflection coefficient we deduce that the variance goes to zero.

Note that an integral over frequency (ensured by the time domain nature of time-reversal) is needed for the stabilization or the self-averaging of the refocused pulse. Applications of this result to the problem of the location of the source will be discussed in Section 6.

5. The random case with an interior point source

In this section we assume that the source is below the surface ($z_s < 0$). The time-reversal strategy is the same as in the previous section, we obtain analogous results but the computations are more complicated and do not lead to fully explicit formulas such as the ones presented in Theorem 4.1.

5.1. The stationary phase in the random case

We consider the P_1 term in the representation of the longitudinal velocity (23) with arbitrary z_s (depth of the source) and z (depth of the observation point). The other terms can be treated in the same way and we will collect and discuss all the contributions in Section 5.3. Once again, the generalized reflection coefficients at two different slowness vectors are correlated only if the frequencies and moduli of the slowness vectors are close to each other at order ε. We accordingly perform the same change of variables as in Section 4, so that the representation of the P_1

term of the longitudinal velocity field becomes

$$u^{(1)}_{\mathrm{TR}}(t,\mathbf{x}=r_0\mathbf{e}_{\theta_0},z) = -\frac{1}{(2\pi)^6\varepsilon}\int\int \frac{H_0(\mu\mathbf{e}_\theta,\mu\mathbf{e}_{\theta'})}{4\sqrt{I_0(\mu)}}\bar{\hat{G}}_1(-h)\hat{G}_2(\omega\mu(\mathbf{e}_\theta+\mathbf{e}_{\theta'}))\bar{S}_b(\omega,\mu\mathbf{e}_{\theta'})$$
$$\times \mathrm{e}^{\mathrm{i}\phi(\omega,\mu,\theta,\theta')/\varepsilon}\,\mathrm{e}^{(\mathrm{i}/2)(h(t-t_\mathrm{s})+(\lambda\omega+h\mu)[r_\mathrm{s}\cos(\theta_\mathrm{s}-\theta')-r_0\cos(\theta_0-\theta)]-[h\zeta_0(\mu)+\omega\zeta_0'(\mu)\lambda](z+z_\mathrm{s}))}$$
$$\times \bar{R}_\mathrm{g}\left(\omega+\frac{\varepsilon h}{2},\mu+\frac{\varepsilon\lambda}{2},z_\mathrm{s}\right)R_\mathrm{g}(\omega-\frac{\varepsilon h}{2},\mu-\frac{\varepsilon\lambda}{2},z)\omega^4\mu^2\,\mathrm{d}\lambda\,\mathrm{d}h\,\mathrm{d}\omega\,\mathrm{d}\mu\,\mathrm{d}\theta\,\mathrm{d}\theta', \quad (27)$$

where $\zeta_0'(\mu) = -\mu/\zeta_0(\mu)$ and the rapid phase is

$$\phi(\omega,\mu,\theta,\theta') = \omega[-(t_\mathrm{s}+t)+\mu(r_\mathrm{s}\cos(\theta_\mathrm{s}-\theta')+r_0\cos(\theta_0-\theta))+\zeta_0(\mu)(z-z_\mathrm{s})].$$

As in Section 4 we first apply the stationary phase method and we will deal with the random part of the integral (the product of the two generalized reflection coefficients) in a second step. The variables of the rapid phase are ω, μ, θ, and θ'. We assume that $\mathbf{r}_\mathrm{s} \neq 0$, that is the case where the mirror is not directly above the source. There are several remarkable configurations.

(1) If $c_0^2(t+t_\mathrm{s})^2 \neq (r_\mathrm{s}-r_0)^2+(z-z_\mathrm{s})^2$, then there is no stationary map.
(2) If $c_0^2(t+t_\mathrm{s})^2 = (r_\mathrm{s}-r_0)^2+(z-z_\mathrm{s})^2$ and $z \neq z_\mathrm{s}$, then there exists one map of stationary points which is three-dimensional (i.e. the map is concentrated around critical values of θ, θ', and μ with no restriction on ω). The stationary phase method gives an effective value for the integral (27) which is of order $\varepsilon^{3/2}$ and consequently contributes to a term of order $\varepsilon^{1/2}$ to $u^{(1)}_{\mathrm{TR}}$.
(3) If $t+t_\mathrm{s}=0$, $r_0=r_\mathrm{s}$, and $z=z_\mathrm{s}$, then there exist two maps of stationary points corresponding to (I) $\theta'=\theta_\mathrm{s}$ and $\theta=\theta_0+\pi$, (II) $\theta'=\theta_\mathrm{s}+\pi$ and $\theta=\theta_0$ with no restriction on ω and μ. Because of the additional degeneracy in μ, these two stationary maps are two-dimensional and the stationary phase method gives an effective value for the integral which is of order ε and consequently only this configuration contributes to a term of order 1 to $u^{(1)}_{\mathrm{TR}}$. In other words, this component of the time reversed wave is only observed at the right time $-t_\mathrm{s}$, at the right depth z_s, and on the ring with radius r_s. We accordingly consider an observation time t close to $-t_\mathrm{s}$, and an observation point $(\mathbf{x},z)$ which is such that z is close to z_s and the modulus of $\mathbf{x}$ is close to r_s. We do so by writing $t=-t_\mathrm{s}+\varepsilon\mathcal{T}$, $\mathbf{x}=r_\mathrm{s}\mathbf{e}_{\theta_0}+\varepsilon\mathcal{R}\mathbf{e}_\phi$, and $z=z_\mathrm{s}+\varepsilon\mathcal{Z}$. We get that, to leading order in ε, the P_1 term of the longitudinal velocity field consists of the sum of two terms corresponding to the contributions of the two maps of stationary points (I and II)

$$u^{(1)}_{\mathrm{TR}}(t,\mathbf{x},z) = u^{(1,\mathrm{I})}_{\mathrm{TR}}(t,\mathbf{x},z)+u^{(1,\mathrm{II})}_{\mathrm{TR}}(t,\mathbf{x},z),$$
$$u^{(1,\mathrm{I})}_{\mathrm{TR}}(t,\mathbf{x},z) = -\frac{1}{2^7\pi^5 r_\mathrm{s}}\int\int \frac{H_0(-\mu\mathbf{e}_{\theta_0},\mu\mathbf{e}_{\theta_\mathrm{s}})}{\sqrt{I_0(\mu)}}\bar{\hat{G}}_1(-h)\hat{G}_2(\omega\mu(\mathbf{e}_{\theta_\mathrm{s}}-\mathbf{e}_{\theta_0}))\bar{S}_b(\omega,\mu\mathbf{e}_{\theta_\mathrm{s}})$$
$$\times \mathrm{e}^{\mathrm{i}(-\omega\mathcal{T}-\omega\mu\mathcal{R}\cos(\theta_0-\phi)+\omega\zeta_0(\mu)\mathcal{Z}-ht_\mathrm{s}+r_\mathrm{s}(\lambda\omega+h\mu)-[h\zeta_0(\mu)+\omega\zeta_0'(\mu)\lambda]z_\mathrm{s})}$$
$$\times \bar{R}_\mathrm{g}\left(\omega+\frac{\varepsilon h}{2},\mu+\frac{\varepsilon\lambda}{2},z_\mathrm{s}\right)R_\mathrm{g}\left(\omega-\frac{\varepsilon h}{2},\mu-\frac{\varepsilon\lambda}{2},z_\mathrm{s}+\varepsilon\mathcal{Z}\right)\omega^3\mu\,\mathrm{d}\lambda\,\mathrm{d}h\,\mathrm{d}\omega\,\mathrm{d}\mu,$$
$$u^{(1,\mathrm{II})}_{\mathrm{TR}}(t,\mathbf{x},z) = -\frac{1}{2^7\pi^5 r_\mathrm{s}}\int\int \frac{H_0(\mu\mathbf{e}_{\theta_0},-\mu\mathbf{e}_{\theta_\mathrm{s}})}{\sqrt{I_0(\mu)}}\bar{\hat{G}}_1(-h)\hat{G}_2(\omega\mu(\mathbf{e}_{\theta_0}-\mathbf{e}_{\theta_\mathrm{s}}))\bar{S}_b(\omega,-\mu\mathbf{e}_{\theta_\mathrm{s}})$$
$$\times \mathrm{e}^{\mathrm{i}(-\omega\mathcal{T}+\omega\mu\mathcal{R}\cos(\theta_0-\phi)+\omega\zeta_0(\mu)\mathcal{Z}-ht_\mathrm{s}-r_\mathrm{s}(\lambda\omega+h\mu)-[h\zeta_0(\mu)+\omega\zeta_0'(\mu)\lambda]z_\mathrm{s})}$$
$$\times \bar{R}_\mathrm{g}\left(\omega+\frac{\varepsilon h}{2},\mu+\frac{\varepsilon\lambda}{2},z_\mathrm{s}\right)R_\mathrm{g}\left(\omega-\frac{\varepsilon h}{2},\mu-\frac{\varepsilon\lambda}{2},z_\mathrm{s}+\varepsilon\mathcal{Z}\right)\omega^3\mu\,\mathrm{d}\lambda\,\mathrm{d}h\,\mathrm{d}\omega\,\mathrm{d}\mu.$$

This integral representation of the signal shows that the autocorrelation function of the generalized reflection coefficient defined by (17) plays a key role.

5.2. Asymptotics of the first moment of $u_{\mathrm{TR}}^{(1)}$

The computation of the expectation of the P_1 term of the integral representation of $u_{\mathrm{TR}}^{(1)}$ is reduced to the computation of the quantity

$$U_{\mathrm{g}}^{\varepsilon} = \mathbb{E}\left[\bar{R}_{\mathrm{g}}\left(\omega + \frac{\varepsilon h}{2}, \mu + \frac{\varepsilon\lambda}{2}, z_{\mathrm{s}}\right) R_{\mathrm{g}}\left(\omega - \frac{\varepsilon h}{2}, \mu - \frac{\varepsilon\lambda}{2}, z_{\mathrm{s}} + \varepsilon\mathcal{Z}\right)\right].$$

Using the representation (19) of the generalized coefficient R_{g} in terms of the usual reflection and transmission coefficients, we obtain that

$$U_{\mathrm{g}}^{\varepsilon} = \sum_{n,m=0}^{\infty} \mathbb{E}[\bar{R}^{n+1}\ R^{m+1}\ \tilde{R}^{n}\ \tilde{T}\ \bar{\tilde{R}}^{m}\ \bar{\tilde{T}}],$$

where $\bar{R}^{n+1}$ is evaluated at $(\omega + \varepsilon h/2, \mu + \varepsilon\lambda/2, -L, z_{\mathrm{s}})$, R^{m+1} is evaluated at $(\omega - \varepsilon h/2, \mu - \varepsilon\lambda/2, -L, z_{\mathrm{s}} + \varepsilon\mathcal{Z})$, $\tilde{R}^{n}\tilde{T}$ is evaluated at $(\omega + \varepsilon h/2, \mu + \varepsilon\lambda/2, z_{\mathrm{s}}, 0)$, and $\bar{\tilde{R}}^{n}\bar{\tilde{T}}$ is evaluated at $(\omega - \varepsilon h/2, \mu - \varepsilon\lambda/2, z_{\mathrm{s}} + \varepsilon\mathcal{Z}, 0)$. As $\varepsilon \to 0$ the propagators between $-L$ and z_{s} and between z_{s} and 0 become independent. By continuity with respect to z of the limits of the moments of the reflection and transmission coefficients, the $\varepsilon\mathcal{Z}$ does not play any role in the limit of $U_{\mathrm{g}}^{\varepsilon}$. Accordingly we shall obtain the limit of $U_{\mathrm{g}}^{\varepsilon}$ as $\varepsilon \to 0$ by looking at the limits of $\mathbb{E}[\bar{R}^{n+1}\ R^{m+1}]$ and $\mathbb{E}[\tilde{R}^{n}\ \tilde{T}\ \bar{\tilde{R}}^{m}\ \bar{\tilde{T}}]$. By using the expressions of the limit values for moments of reflection and transmission coefficients, we obtain

$$U_{\mathrm{g}}^{\varepsilon} \xrightarrow{\varepsilon\to 0} \sum_{n=0}^{\infty} \mathrm{e}^{2\mathrm{i}[h\zeta_0(\mu)+\lambda\omega\zeta_0'(\mu)]z_{\mathrm{s}}} \int W_{n+1}(\tau, \omega, \mu)\, \mathrm{e}^{\mathrm{i}\tau H}\, \mathrm{d}\tau \int \tilde{W}_n(\tau, \omega, \mu)\, \mathrm{e}^{\mathrm{i}\tau H}\, \mathrm{d}\tau,$$

where $H = c_0^2\omega\mu\lambda - h(1 - c_0^2\mu^2)$, W_n and $\tilde{W}_n$ are described in Appendix A.2. Substituting the limit of $U_{\mathrm{g}}^{\varepsilon}$ in the integral representations of $u_{\mathrm{TR}}^{(1,I)}$ and $u_{\mathrm{TR}}^{(1,II)}$ we find that

$$\mathbb{E}[u_{\mathrm{TR}}^{(1,\mathrm{I})}(t, \mathbf{x}, z)] \xrightarrow{\varepsilon\to 0} \frac{-1}{2^5\pi^3 r_{\mathrm{s}} c_0^2} \int \frac{H_0(-\mu\mathbf{e}_{\theta_0}, \mu\mathbf{e}_{\theta_{\mathrm{s}}})}{\sqrt{I_0(\mu)}} \hat{G}_2(\omega\mu(\mathbf{e}_{\theta_{\mathrm{s}}} - \mathbf{e}_{\theta_0}))\bar{S}_b(\omega, \mu\mathbf{e}_{\theta_{\mathrm{s}}})$$
$$\times\, \mathrm{e}^{\mathrm{i}\omega[-\mathcal{T}-\mu\mathcal{R}\cos(\theta_0-\phi)+\zeta_0(\mu)\mathcal{Z}]} G_1\left(t_{\mathrm{s}} - \frac{r_{\mathrm{s}}}{c_0^2\mu}\right) W_{g,+}\left(\frac{-r_{\mathrm{s}} + (\mu/\zeta_0(\mu))z_{\mathrm{s}}}{\mu c_0^2}\right) \omega^2\, \mathrm{d}\mu\, \mathrm{d}\omega,$$
$$\mathbb{E}[u_{\mathrm{TR}}^{(1,\mathrm{II})}(t, \mathbf{x}, z)] \xrightarrow{\varepsilon\to 0} \frac{-1}{2^5\pi^3 r_{\mathrm{s}} c_0^2} \int \frac{H_0(\mu\mathbf{e}_{\theta_0}, -\mu\mathbf{e}_{\theta_{\mathrm{s}}})}{\sqrt{I_0(\mu)}} \hat{G}_2(\omega\mu(\mathbf{e}_{\theta_0} - \mathbf{e}_{\theta_{\mathrm{s}}}))\bar{S}_b(\omega, -\mu\mathbf{e}_{\theta_{\mathrm{s}}})$$
$$\times\, \mathrm{e}^{\mathrm{i}\omega[-\mathcal{T}+\mu\mathcal{R}\cos(\theta_0-\phi)+\zeta_0(\mu)\mathcal{Z}]} G_1\left(t_{\mathrm{s}} + \frac{r_{\mathrm{s}}}{c_0^2\mu}\right) W_{g,+}\left(\frac{r_{\mathrm{s}} + (\mu/\zeta_0(\mu))z_{\mathrm{s}}}{\mu c_0^2}\right) \omega^2\, \mathrm{d}\mu\, \mathrm{d}\omega,$$

where $t = -t_s + \varepsilon\mathcal{T}$, $\mathbf{x} = r_s\mathbf{e}_{\theta_0} + \mathcal{R}\mathbf{e}_\phi$, $z = z_s + \varepsilon\mathcal{Z}$, and

$$W_{g,+}(\tau,\omega,\mu) = \sum_{n=0}^{\infty}[W_{n+1}(\cdot,\omega,\mu,-L,z_s) * \tilde{W}_n(\cdot,\omega,\mu,z_s,0)](\tau).$$

It is clear from the transport equations (A.1) and (A.6) that W_n and $\tilde{W}_n$ vanish for $\tau < 0$ (see also [1]), so that $W_{g,+}$ also vanishes for $\tau < 0$. As a consequence the limit of $\mathbb{E}[u_{\mathrm{TR}}^{(1,I)}(t,\mathbf{x},z)]$ is zero, and only the second map contributes to the expected value of $u_{\mathrm{TR}}^{(1)}$.

5.3. Other components to the first moment of u_{TR}

We have just addressed the P_1 term of the integral representation (23) of u_{TR}. We now consider the three other terms P_2, P_3, and P_4. The terms $u_{\mathrm{TR}}^{(2)}$ and $u_{\mathrm{TR}}^{(4)}$ associated with P_2 and P_4 have no stationary point because z and z_s appear with the same signs in their fast phases. Consequently these two terms do not contribute to the limit value of u_{TR} as $\varepsilon \to 0$. We now address the term $u_{\mathrm{TR}}^{(3)}$ associated with P_3 given by Eq. (23). In this case, the generalized transmission coefficients at two different slowness vectors are always correlated. Consequently the domain of integration contributing to the value of the integral (23) is not restricted to an ε-neighborhood of the diagonal $\mu' \simeq \mu$. We thus split the domain of integration into two parts. The first part corresponds to a sub-domain which is an ε-neighborhood of the diagonal. It can be treated as in the previous section where we dealt with the P_1 term. The second part contains the non-diagonal contribution to the integral which captures the coherent propagating front as described below.

5.3.1. Diagonal contribution

The integral representation of the diagonal contribution $u_{\mathrm{TR}}^{(3,\mathrm{diag})}$ is similar to Eq. (27), but involves the product of two generalized transmission coefficients and appropriate phases. The random component can be expanded in terms of the usual transmission and reflection coefficients as

$$\bar{T}_g T_g = \sum_{n,m=0}^{\infty} \bar{R}^n R^m \tilde{R}^n \tilde{T} \bar{\tilde{R}}^m \bar{\tilde{T}}.$$

Following the same strategy as in the previous sections and using the asymptotic analysis for the expectation of the moments of transmission-reflection coefficients presented in Appendix A.2, we get that the only configuration leading to an expected value of order one for $u_{\mathrm{TR}}^{(3,\mathrm{diag})}$ is obtained when the observation coordinates t, z, and $|\mathbf{x}|$ are in an ε-neighborhood of $-t_s$ and r_s, and z_s, respectively. More precisely, taking $t = -t_s + \varepsilon\mathcal{T}$, $\mathbf{x} = r_s\mathbf{e}_{\theta_0} + \varepsilon\mathcal{R}\mathbf{e}_\phi$, and $z = z_s + \varepsilon\mathcal{Z}$, we get that

$$\mathbb{E}[u_{\mathrm{TR}}^{(3,\mathrm{diag})}(t,\mathbf{x},z)] \xrightarrow{\varepsilon\to 0} \frac{-1}{2^5\pi^3 r_s c_0^2}\int \frac{H_0(\mu\mathbf{e}_{\theta_0},-\mu\mathbf{e}_{\theta_s})}{\sqrt{I_0(\mu)}}\hat{G}_2(\omega\mu(\mathbf{e}_{\theta_0}-\mathbf{e}_{\theta_s}))\bar{S}_a(\omega,-\mu\mathbf{e}_{\theta_s})$$
$$\times\, \mathrm{e}^{\mathrm{i}\omega[-\mathcal{T}-\mu\mathcal{R}\cos(\theta_0-\phi)-\zeta_0(\mu)\mathcal{Z}]} G_1\left(t_s + \frac{r_s}{c_0^2\mu}\right) W_{g,-}\left(\frac{r_s + (\mu/\zeta_0(\mu))z_s}{\mu c_0^2}\right)\omega^2\,\mathrm{d}\mu\,\mathrm{d}\omega,$$

where

$$W_{g,-}(\tau,\omega,\mu) = \sum_{n=0}^{\infty}[W_n(\cdot,\omega,\mu,-L,z-s) * \tilde{W}_n(\cdot,\omega,\mu,z-s,0)](\tau).$$

5.3.2. Off-diagonal contribution

The off-diagonal contribution $u_{\rm TR}^{(3,\rm off)}$ corresponds to the time reversal of the coherent front. It has been analyzed in detail in [12] in the case of time-reversal in transmission, so by a simple generalization using the moment analysis presented in Appendix A.1, one can deduce that the coherent time-reversed front wave propagates like a spherical wave around $z^2+|\mathbf{x}|^2=c_0^2(t-t_c)^2$ and $t_c=-t_{\rm s}-\sqrt{z_{\rm s}^2+r_{\rm s}^2}/c_0$. This analysis can be viewed as a straightforward extension of the O'Doherty–Anstey (ODA) theory (see Appendix A.3). More precisely, if the mirror is pointwise so that $\hat{G}_2(\mathbf{k})\equiv\hat{g}_2$, then $u_{\rm TR}^{(3,\rm off)}$ converges in distribution as $\varepsilon\to 0$ to

$$u_{\rm TR}^{\rm coh}(t,\mathbf{x},z)=G_1(-t_c)u_{\rm TR,\mathbf{x},z}^{\rm hom}*K_{{\rm ODA},\mathbf{x},z}\left(\frac{\sqrt{z^2+|\mathbf{x}|^2}-\sqrt{z_{\rm s}^2+|\mathbf{x}_{\rm s}|^2}}{c_0\varepsilon}-\frac{t+t_{\rm s}}{\varepsilon}\right),$$

where $u_{\rm TR}^{\rm hom}$ is the front shape in homogeneous medium computed in Section 3

$$u_{\rm TR,\mathbf{x},z}^{\rm hom}(t)=-\frac{\hat{g}_2}{(4\pi)^2\rho_0c_0^3}\frac{(\mathbf{x}\cdot\mathbf{x}_{\rm s}+zz_{\rm s})z}{\sqrt{r_{\rm s}^2+z_{\rm s}^2}^3\sqrt{|\mathbf{x}|^2+z^2}^3}[\mathbf{x}_{\rm s}\cdot\mathbf{f}_{\mathbf{x}}''(t)+z_{\rm s}f_z''(t)]. \tag{28}$$

$K_{{\rm ODA},\mathbf{x},z}$ is the convolution of two standard ODA kernels. Its Fourier transform is

$$\hat{K}_{{\rm ODA},\mathbf{x},z}(\omega)=\exp\left(\mathrm{i}[\sqrt{\gamma(\omega,\mu_1)}B_z-\sqrt{\gamma(\omega,\mu_2)}B_{z_{\rm s}}]+\frac{\gamma(\omega,\mu_1)z+\gamma(\omega,\mu_2)z_{\rm s}}{2}\right) \tag{29}$$

with $\mu_1=(1/c_0)(|\mathbf{x}|/\sqrt{|\mathbf{x}|^2+z^2})$, $\mu_2=(1/c_0)(r_{\rm s}/\sqrt{r_{\rm s}^2+z_{\rm s}^2})$, B is a Brownian motion, and γ is given by (A.2).

The shape of the front is deterministic and results from a first spreading due to the propagation from the source to the mirror cumulated with a second spreading due to the propagation from the mirror to the observation point. The random medium also imposes a random shift which cancels out if the observation point is taken on the ring $z=z_{\rm s}$ and $|\mathbf{x}|=r_{\rm s}$.

5.4. Summary

We sum up the previous results in the next theorem. We assume a point mirror so that $\hat{G}_2(\mathbf{k})=\hat{g}_2$. We also assume the generic case where the mirror is not exactly above the source, that is to say $r_{\rm s}\neq 0$. We consider the time reversed wave and observe it in an ε-neighborhood of an arbitrary observation point (t_0,r_0,z_0). Three types of configurations can be distinguished. The first case (a) corresponds to an observation point outside of the support of the spherical front wave. The observed field has a vanishing amplitude. The second case (b) corresponds to an observation point on the support of the spherical front wave but outside the refocusing ring. The observed field is the coherent wave front described in terms of the ODA kernel. The third case (c) corresponds to an observation point on the refocusing ring. The observed velocity field consists in the superposition of the coherent wave front and of the refocusing of the recorded incoherent coda waves.

Theorem 5.1. *Let us denote* $t_c=-t_{\rm s}-\sqrt{r_{\rm s}^2+z_{\rm s}^2}/c_0$.

(a) *If* $c_0^2(t_0-t_c)^2\neq r_0^2+z_0^2$, *then, for any* $\mathcal{T}_0>0$, $\mathcal{R}_0>0$, $\mathcal{Z}_0>0$, *and* $\delta>0$, *we have*

$$\mathbb{P}\left(\sup_{|\mathcal{T}|\le\mathcal{T}_0,|\mathcal{R}|\le\mathcal{R}_0,\theta_0\in[0,2\pi),|\mathcal{Z}|\le\mathcal{Z}_0}|u_{\rm TR}(t_0+\varepsilon\mathcal{T},(r_0+\varepsilon\mathcal{R})\mathbf{e}_{\theta_0},z_0+\varepsilon\mathcal{Z})|>\delta\right)\xrightarrow{\varepsilon\to 0}0.$$

(b) *If* $c_0^2(t_0 - t_c)^2 = r_0^2 + z_0^2$ *and* $t_0 \neq -t_s$, *then for any* $\mathcal{T}_0 > 0$, $\mathcal{R}_0 > 0$, *and* $\mathcal{Z}_0 > 0$, *we have the following convergence in distribution*

$$(u_{\mathrm{TR}}(t_0 + \varepsilon\mathcal{T}, (r_0 + \varepsilon\mathcal{R})\mathbf{e}_{\theta_0}, z_0 + \varepsilon\mathcal{Z}))_{|\mathcal{T}|\leq\mathcal{T}_0, |\mathcal{R}|\leq\mathcal{R}_0, \theta_0\in[0,2\pi), |\mathcal{Z}|\leq\mathcal{Z}_0} \tag{30}$$

$$\xrightarrow{\varepsilon\to 0} G_1(-t_c)[u^{\mathrm{hom}}_{\mathrm{TR}, r_0\mathbf{e}_{\theta_0}, z_0} * K_{\mathrm{ODA}, r_0\mathbf{e}_{\theta_0}, z_0}]\left(\frac{r_0\mathcal{R} + z_0\mathcal{Z}}{c_0\sqrt{r_0^2 + z_0^2}} - \mathcal{T}\right), \tag{31}$$

where $u^{\mathrm{hom}}_{\mathrm{TR}}$ *is the front shape in homogeneous medium given by (28) and* K_{ODA} *is the random kernel given by (29).*

(c) *If* $c_0^2(t_0 - t_c)^2 = r_0^2 + z_0^2$, $t_0 = -t_s$, *and* $z_0 = z_s$ (so $r_0 = r_s$), *then for any* $\mathcal{T}_0 > 0$, $\mathcal{R}_0 > 0$, $\mathcal{Z}_0$, *and* $\delta > 0$, *we have*

$$\mathbb{P}\left(\sup_{|\mathcal{T}|\leq\mathcal{T}_0, |\mathcal{R}|\leq\mathcal{R}_0, \theta_0\in[0,2\pi), |\mathcal{Z}|\leq\mathcal{Z}_0} |u_{\mathrm{TR}}(t_0 + \varepsilon\mathcal{T}, (r_0 + \varepsilon\mathcal{R})\mathbf{e}_{\theta_0}, z_0 + \varepsilon\mathcal{Z}) - U_{\mathrm{TR}}(\mathcal{T}, \mathcal{R}, \mathcal{Z})| > \delta\right) \xrightarrow{\varepsilon\to 0} 0,$$

where U_{TR} *is the deterministic pulse shape*

$$\begin{aligned}
U_{\mathrm{TR}}(\mathcal{T}, \mathcal{R}, \mathcal{Z}) &= u^{\mathrm{hom}}_{\mathrm{TR}, r_s\mathbf{e}_{\theta_0}, z_s} * K_0\left(\frac{r_s\mathcal{R} + z_s\mathcal{Z}}{c_0\sqrt{r_s^2 + z_s^2}} - \mathcal{T}\right) \\
&\quad + \frac{1}{(2\pi)^3}\int \hat{K}^+(\omega, \mu)\left[\frac{\mu}{2\rho_0}\mathbf{e}_{\theta_s}\cdot\bar{\hat{\mathbf{f}}}_{\mathbf{x}}(\omega) + \frac{1}{2I_0(\mu)}\bar{\hat{f}}_z(\omega)\right] \mathrm{e}^{\mathrm{i}\omega(\mu\mathcal{R} - \mathcal{T} + \zeta_0(\mu)\mathcal{Z})}\omega^2\,\mathrm{d}\omega\,\mathrm{d}\mu \\
&\quad + \frac{1}{(2\pi)^3}\int \hat{K}^-(\omega, \mu)\left[\frac{\mu}{2\rho_0}\mathbf{e}_{\theta_s}\cdot\bar{\hat{\mathbf{f}}}_{\mathbf{x}}(\omega) + \frac{1}{2I_0(\mu)}\bar{\hat{f}}_z(\omega)\right] \mathrm{e}^{\mathrm{i}\omega(\mu\mathcal{R} - \mathcal{T} - \zeta_0(\mu)\mathcal{Z})}\omega^2\,\mathrm{d}\omega\,\mathrm{d}\mu,
\end{aligned}$$

$$\hat{K}_0(\omega) = G_1(-t_c)\exp\left(-\frac{\gamma_0\omega^2(r_s^2 + z_s^2)}{2c_0^2|z_s|}\right),$$

$$\hat{K}^{\pm}(\omega, \mu) = G_1\left(t_s + \frac{r_s}{c_0^2\mu}\right) W_{g,\pm}\left(\frac{r_s + (\mu/\zeta_0(\mu))z_s}{\mu c_0^2}\right)\frac{H_0(\mu\mathbf{e}_{\theta_0}, -\mu\mathbf{e}_{\theta_s})}{2c_0^2 r_s}.$$

Note that the kernels K_0 and $K^{\pm}$ depend only on the integrated covariance of the fluctuations of the medium γ_0. An explicit expression for H_0 is given by (26). The picture is qualitatively the same for the time-reversed transverse velocity and pressure fields and we do write the complete expressions which are rather long. The proof of the theorem follows the same line as the one of Theorem 4.1. In Sections 5.2–5.3 we have derived the asymptotics of the expected value of the refocused pulse on the ring. To get the deterministic nature of the limit, it remains to compute the variance of the refocused field. It involves the computation of the forth moments of the generalized reflection and transmission coefficients. This is done again by using Appendix A.2.

6. Source identification

In this section we indicate briefly how the results derived above are useful in solving the inverse source problem. We assume that we are in the configuration shown in Fig. 1. The source S emits a short pulse from an unknown location (x_s, z_s) at an unknown time t_s. Our objective is to identify these unknowns and the shape of the pulse

assuming that we observe the signal that emerges at the surface at a receiver with a small spatial extent. Such a problem can be encountered in various contexts, such as geophysics [19] or oceanography [17]. The small aperture of the receiver in our configuration makes the identification of the source location challenging by standard methods. The known position of the receiver is chosen as the origin. We assume that the medium is randomly layered on a fine scale and that we know the particular realization "seen" by the wave. Our strategy is to perform a synthetic time-reversal experiment meaning that we numerically solve the wave equation and compute the time reversed wave field described in the paper. In the regime of our asymptotic analysis the time reversed wave will exhibit a propagating spherical front wave and, at a precise time, an additional ring located at the depth of the source and passing through the source point. This is precisely stated in Theorem 5.1. Note that the re-propagated front wave can be computed by simply observing the first arrival at the receiver but it does not contain any information on the source location and time of emission. In contrast the use of the incoherent coda of the wave and time-reversal techniques lead to an information about the depth of the source, its lateral distance from the mirror, and its emission time. The shape of the source pulse can then be reconstructed precisely by using the shape of the first arrival and a deconvolution process through the ODA kernel (A.7) described in Appendix A.3. Furthermore this identification can also be performed with the presence of additional noisy sources emitting at the surface. By the results of Section 5.4 the additional sources only produce refocused fields at the surface. The refocused ring is therefore produced only by the source inside the domain.

If only the statistical properties of the medium are known, but not the particular realization, the strategy would be to estimate the kernel from the measure of the wave emerging at the receiver and the computation of the local autocorrelation function of the signal [1]. This is a difficult problem which is a topic of future research. In other contexts such as underwater acoustics [13] the medium is not known but time-reversal can be performed physically. The refocusing properties proved in this paper in an ideal layered setting can be used for telecommunication purposes.

7. Numerical illustration

In this section we present a two-dimensional numerical illustration of the theory developed in this paper. Time-reversal refocusing is a phenomenon that takes place in different wave applications. Hence to illustrate its range of applicability we perform numerical experiments using a shallow water model. The linear two-dimensional shallow water equations [21] are given as

$$U_t = -g\eta_x + f_x, \qquad V_t = -g\eta_y + f_y, \qquad \eta_t + (hU)_x + (hV)_y = 0, \tag{32}$$

where $U(x, y, t)$ and $V(x, y, t)$ are vertically z-averaged velocities. The free surface wave elevation is denoted by $\eta(x, y, t)$. This term represents the excess pressure about the undisturbed free surface $z \equiv 0$. The randomly layered medium is represented by the disordered bottom topography through $h(x, y)$. By using the flux vector $\boldsymbol{\psi} = (\psi^u, \psi^v)^{\mathrm{T}} \equiv (hU, hV)^{\mathrm{T}}$ the correspondence between the shallow water and the acoustic model is more easily established: $\boldsymbol{\psi}_t - gh\nabla\eta = 0$, $\eta_t + \nabla \cdot \boldsymbol{\psi} = 0$. The simulations refer to model (32). Details of the Lagrangian numerical scheme are provided in [5]. We have adapted the code in order to have the data imposed through the velocity forcing terms. The setup for the numerical experiments is given in Fig. 7(a).

The random medium slab is located at $x > 0$. The source location is at $(x_{\mathrm{S}}, y_{\mathrm{S}}) = (10, 0)$ and we place two time-reversal (point) mirrors at $(x_{\mathrm{M1}}, y_{\mathrm{M1}}) = (0, 4)$ and $(x_{\mathrm{M2}}, y_{\mathrm{M2}}) = (0, -4)$ corresponding to the surface location of the acoustic slab, here given by $x \equiv 0$. The velocity sources are such that both f_x and f_y have a Gaussian $f(t) = \exp(-(t - t_{\mathrm{s}})^2/0.02)$ profile of duration approximately equal to 1/3 time units. The randomly layered topography has a correlation length of 0.1 with 40% fluctuations about the undisturbed depth. A nearly circular, pulse shaped, wave front propagates over the random medium and time histories (for the velocity fields) are recorded at mirror M1 and mirror M2, as displayed in Fig. 8. We observe the wave front arriving, at approximately $t = 10.8$ followed

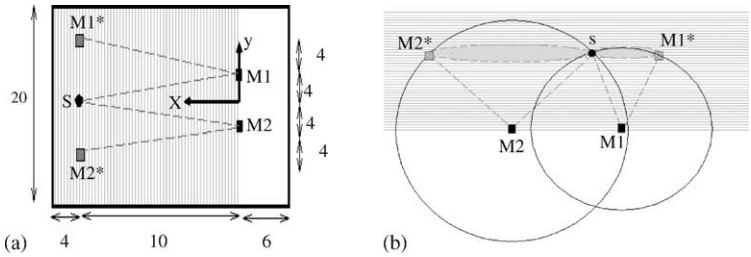

Fig. 7. (a) Schematic setup for the randomly layered topography. The source point **S** is at $(x_S, y_S) = (10, 0)$ corresponding to nodes (1600, 1000). The shaded area represents the randomly layered medium. (b) Schematic graph for the wave fronts (centered at the mirrors M1 and M2) together with the refocusing rings (dashed curves). Each ring is at the base of a three-dimensional cone defined by the corresponding triplet (M, M*, S). The shaded area highlights the *xz* circle/ring intersecting the *xy* plane.

by a fluctuating coda. We time reverse the signals recorded within the time interval [10.8, 18.8]. In the time-reversal experiment these are the corresponding *f*-profiles, now at two Dirac source locations, each corresponding to a point mirror. We repeat the numerical solution procedure and two pulse shaped fronts propagate towards the source location.

In all numerical experiments we use a 2000×2000 spatial grid with $\Delta x = \Delta y = 0.01$. The time stepping parameter is $\Delta t = 0.0005$. These were chosen due to accuracy and not for stability reasons [5]. We have used reflecting boundary conditions. However the waves reflected from the side walls stay away from our region of interest during the time interval of our study.

As mentioned before the time reversed signals, indicated in Fig. 8, are back-propagated from the two mirrors. The theory predicts two refocusing rings since we have two mirrors. A schematic picture for the rings' configuration

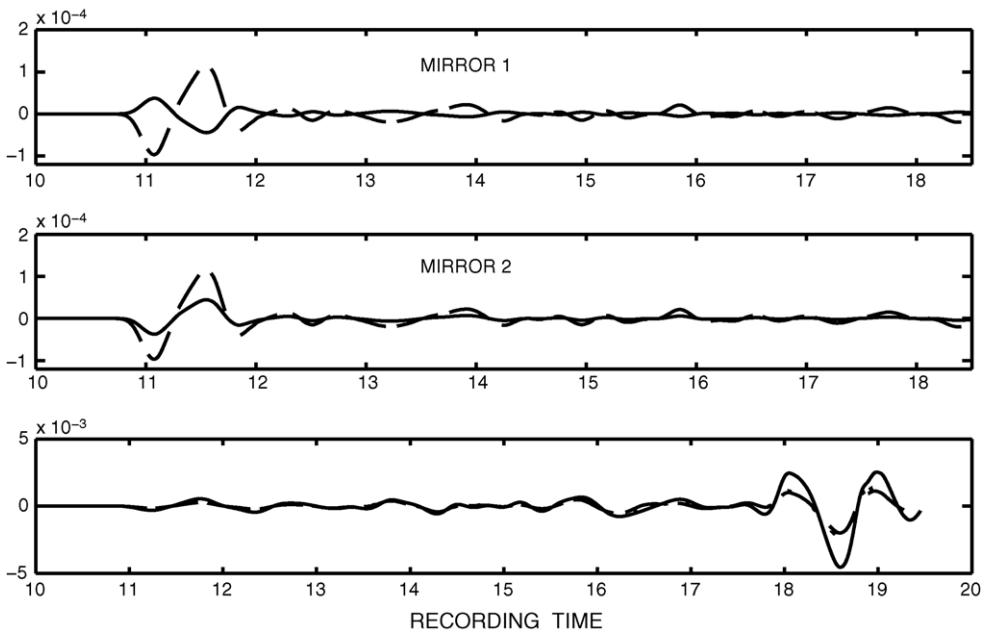

Fig. 8. (Top and middle) Recorded signals at the two mirrors: dashed line represents *U* while the solid line represents *V*. (Bottom) time history for the wave elevation η at the source location (solid line), at the image point M1* (dashed line) and M2* (dotted line).

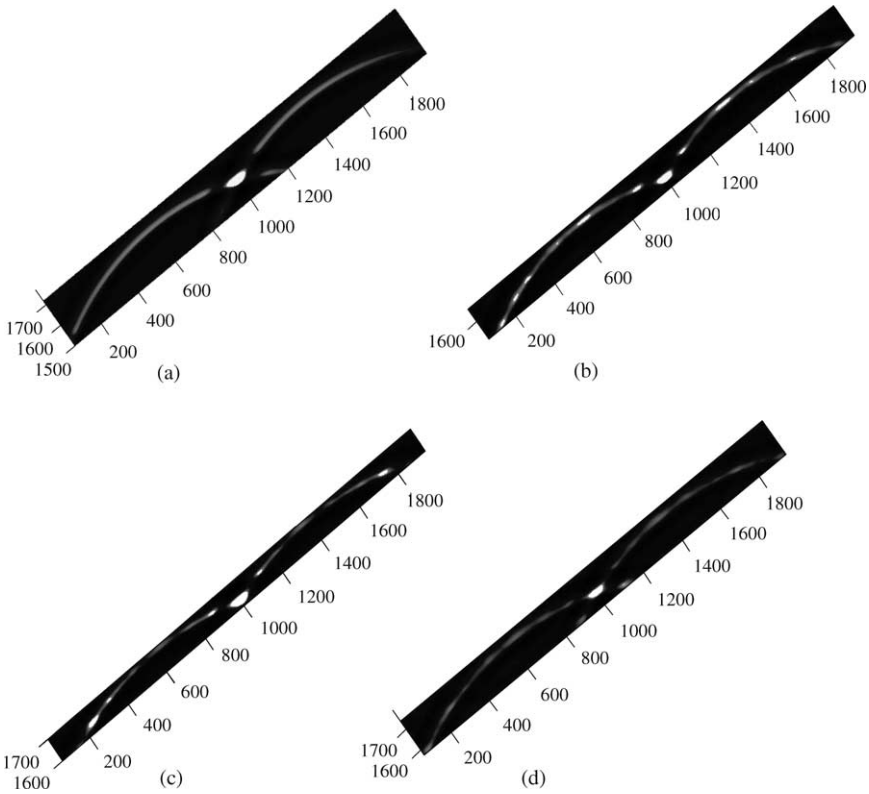

Fig. 9. Node numbers indicated according to Fig. 7. (a) Homogeneous medium. (b) Random medium. Snapshot (at $t = 18.25$) before the critical time t_c. (c) Refocusing observed at three bright spots: source point (spot at the middle) and two image points. Snapshot at $t_c = 18.80$. (d) Snapshot at $t = 18.95 > t_c$.

is given in Fig. 7(b). In our particular example both rings will have the same radius since the mirrors are positioned symmetrically with respect to the source. By no means this is a special configuration. As indicated by a grey disk in Fig. 7(b), in a two-dimensional problem each refocusing ring will be identified by two points, namely the intersection of the ring with the *xy* plane. The rings, corresponding to each mirror, will coincide (and add up) at the source point but will also define *image points* corresponding to the other point of each ring's cross-section with the *xy* plane. We will label these image points as M1* and M2* in connection with the notation of the corresponding point mirror. In Fig. 7 they are indicated by two grey squares near the source point. At the bottom graph of Fig. 8 we have the time history at the source location and also at the image points M1* and M2*. As expected the front is the second derivative of a Gaussian (namely of $f(t)$). For better visualization of refocusing, along the front's largest (absolute) value, from now on we will graph minus the value of the wave elevation. In high contrast the bright spots will indicate regions where the absolute value of the wave amplitude is more intense.

In Fig. 9(a) we consider time-reversal in a homogeneous medium. The time reversed data has been emitted from the two point mirrors and the two fronts have reached the source location. Obviously there are no image points, since we are in a homogeneous medium. The central bright spot is simply due to the superposition of the two fronts. Note that it is impossible to locate the source. The bright spot propagates (unchanged) along the *x*-axis.

In Fig. 9(b) we have the wavefront right before refocusing takes place. We can observe a noticeable middle bright point. In Fig. 9(c), at the critical time, we now observe a larger bright spot at the original source (refocusing) point and also two smaller bright spots, also along the leading front. In particular the numerical refocusing was better

at (1600, 200) giving a brighter image point. These are the image points mentioned above, and represent the other points where the refocusing rings intersect the *xy* plane. To further highlight this phenomenon we now observe the wavefront at a (slightly) later time in Fig. 9(d). We see that the middle spot is slightly weaker while the image points have disappeared. This clearly indicates refocusing in time and space: beyond the critical time the refocusing ring does not exist anymore. Hence the presence of the image points indicate the precise time where the central bright spot is over the source. This illustrates the fact that the source can be located in the presence of randomness, due to the image points, in contrast to the homogeneous case.

Acknowledgments

This work was supported by ONR grants N00014-02-1-0089, N00014-02-1-0603, N00014-02-1-0090 J. Garnier was supported by the program ACI-NIM-2003-94. A. Nachbin was supported by CNPq/Brazil under grant 300368/96-8. K Sølna was supported by NSF grant DMS0307011 and the Sloan Foundation.

Appendix A. Statistical properties of the reflection and transmission coefficients

A.1. Moments at different slownesses

The values of the moments of the transmission coefficient at different slowness vectors is required in Section 5.3. Let us consider $z_0 < z_1, z_1'$, a central frequency ω, $n + n'$ small relative frequency shifts $h_1, \ldots, h_n, h_1', \ldots h_{n'}'$ and $n + n'$ different slowness vector moduli $\kappa_1 \neq \cdots \neq \kappa_n \neq \kappa_1' \neq \cdots \neq \kappa_{n'}'$. The computation of the limits of the following moments

$$\lim_{\varepsilon\to 0} \mathbb{E}\left[\prod_{j=1}^{n} T(\omega+\varepsilon h_j, \kappa_j, z_0, z_1) \prod_{j=1}^{n'} \overline{T}(\omega+\varepsilon h_j', \kappa_j', z_0, z_1')\right]$$

has been carried out in [6]. It is found that the limits are

$$\mathbb{E}\left[\prod_{j=1}^{n} T_{\text{eff}}(\omega, \kappa_j, z_0, z_1) \prod_{j=1}^{n'} \overline{T}_{\text{eff}}(\omega, \kappa_j', z_0, z_1')\right],$$

$$T_{\text{eff}}(\omega, \kappa, z_0, z) = \exp\left(\mathrm{i}\sqrt{\gamma(\omega,\kappa)}(B_z - B_{z_0}) - \frac{\gamma(\omega,\kappa)(z-z_0)}{2}\right),$$

where B is a Brownian motion and γ is given by (A.2). The same computation carried out with the reflection coefficient leads to the limit

$$\lim_{\varepsilon\to 0} \mathbb{E}\left[\prod_{j=1}^{n} R(\omega+\varepsilon h_j, \kappa_j, z_0, z_1) \prod_{j=1}^{n'} \overline{R}(\omega+\varepsilon h_j', \kappa_j', z_0, z_1')\right] = 0.$$

A.2. Moments at two nearby slownesses and frequencies

Taking the expectation of the integral representation of the time reversed signal shows that the autocorrelation function of the reflection coefficient at two nearby frequencies and slownesses plays a crucial role. As shown in

[1,4] we have, for $z_0 \le z$,

$$\mathbb{E}\left[R^n\left(\omega-\frac{\varepsilon h}{2},\kappa-\frac{\varepsilon\lambda}{2},z_0,z\right)\bar{R}^m\left(\omega+\frac{\varepsilon h}{2},\kappa+\frac{\varepsilon\lambda}{2},z_0,z\right)\right]$$
$$\xrightarrow{\varepsilon\to 0}\begin{cases}\int W_n(\tau,\omega,\kappa,z_0,z)\,\mathrm{e}^{\mathrm{i}\tau[c_0^2\omega\kappa\lambda-h(1-c_0^2\kappa^2)]}\,\mathrm{d}\tau & \text{if } m=n,\\ 0 & \text{otherwise,}\end{cases}$$

where the quantity W_n is obtained through the system of transport equations

$$\frac{\partial W_n}{\partial z}+2n\frac{\partial W_n}{\partial\tau}=\gamma(\omega,\kappa)n^2(W_{n+1}+W_{n-1}-2W_n), \tag{A.1}$$

starting from $W_n(\tau,\omega,\kappa,z_0,z=z_0)=\mathbf{1}_0(n)\delta(\tau)$. The coefficients γ are defined by

$$\gamma(\omega,\kappa)=\frac{\gamma_0\omega^2}{2c_0^4\zeta_0(\kappa)^2},\qquad \gamma_0=\int_0^\infty\mathbb{E}[\nu(0)\nu(z)]\,\mathrm{d}z. \tag{A.2}$$

The case with a large slab ($z_0\to-\infty$) leads to explicit formulas. Applying results from [1] we get that the function W_n converges as $z_0\to-\infty$:

$$W_n(\tau,\omega,\kappa,z_0,z)\xrightarrow{z_0\to-\infty}Q_n\left(\frac{c_0^2\zeta_0(\kappa)}{2}\tau\right)\frac{c_0^2\zeta_0(\kappa)}{2},\qquad Q_n(u)=\frac{\partial}{\partial u}\left[\left(\frac{\gamma(\omega,\kappa)u}{1+\gamma(\omega,\kappa)u}\right)^n\mathbf{1}_{[0,\infty)}(u)\right]. \tag{A.3}$$

Accordingly, the limit value of the expectation of the autocorrelation function of the reflection coefficient is

$$\mathbb{E}\left[R\left(\omega-\frac{\varepsilon h}{2},\kappa-\frac{\varepsilon\lambda}{2},z_0,z\right)\bar{R}\left(\omega+\frac{\varepsilon h}{2},\kappa+\frac{\varepsilon\lambda}{2},z_0,z\right)\right]$$
$$\xrightarrow{\varepsilon\to 0}\int_0^\infty Q_1\left(\frac{c_0^2\zeta_0(\kappa)}{2}\tau\right)\frac{c_0^2\zeta_0(\kappa)}{2}\,\mathrm{e}^{\mathrm{i}\tau[\omega\lambda c_0^2\kappa-hc_0^2\zeta_0(\kappa)^2]}\,\mathrm{d}\tau. \tag{A.4}$$

Denoting $U_j^\varepsilon=R(\omega_j-\varepsilon h_j/2,\mu_j-\varepsilon\lambda_j/2,0)\bar{R}(\omega_j+\varepsilon h_j/2,\mu_j+\varepsilon\lambda_j/2,0)$, it is shown in [4] that for two distinct frequencies $\omega_1\neq\omega_2$ or for distinct $\mu_1\neq\mu_2$ one has

$$|\mathbb{E}[U_1^\varepsilon U_2^\varepsilon]-\mathbb{E}[U_1^\varepsilon]\mathbb{E}[U_2^\varepsilon]|\xrightarrow{\varepsilon\to0}0. \tag{A.5}$$

This decorrelation property is used in this paper to deduce the self-averaging property of the refocused pulse. We also use the fact that the reflection coefficients at distinct frequencies decorrelate as $\varepsilon\to0$ and that their means average to zero to show that the P_2 and P_4 terms of the velocity field are vanishing as $\varepsilon\to0$.

Cross-moments of transmission and reflection coefficients are required in Section 5. Extending once again the results contained in [1], we get that

$$\mathbb{E}\left[R^nT\left(\omega-\frac{\varepsilon h}{2},\kappa-\frac{\varepsilon\lambda}{2},z_0,z\right)\overline{R^mT}\left(\omega+\frac{\varepsilon h}{2},\kappa+\frac{\varepsilon\lambda}{2},z_0,z\right)\right]$$
$$\xrightarrow{\varepsilon\to0}\begin{cases}\int\tilde{W}_n(\tau,\omega,\kappa,z_0,z)\,\mathrm{e}^{\mathrm{i}\tau[c_0^2\omega\kappa\lambda-h(1-c_0^2\kappa^2)]}\,\mathrm{d}\tau & \text{if } m=n,\\ 0 & \text{otherwise,}\end{cases}$$

where the quantity $\tilde{W}_n$ is obtained through the system of transport equations

$$\frac{\partial \tilde{W}_n}{\partial z} + 2n\frac{\partial \tilde{W}_n}{\partial \tau} = \gamma(\omega,\kappa)((n+1)^2\tilde{W}_{n+1} + n^2\tilde{W}_{n-1} - (n^2+(n+1)^2)\tilde{W}_n) \tag{A.6}$$

starting from $\tilde{W}_n(\tau,\omega,\kappa,z_0,z=z_0) = \mathbf{1}_0(n)\delta(\tau)$.

A.3. The coherent pulse front in the random case

In this section we compute the expression of the coherent front pulse that can be recorded at the surface. The source is assumed to be inside the medium, i.e. $z_s < 0$, so the front pulse emitted by the source propagates through the random medium and its propagation is actually governed by the well-known O'Doherty–Anstey (ODA) theory [7,14]. In Section 3 we computed this front pulse (Eq. (24)) as well as the time-reversal of this front pulse (Eq. (25)) in homogeneous medium. We now revisit these results in presence of randomness. In this case the front pulse is modified in two ways. First its shape spreads out in a deterministic way due to multiple scattering. This spreading can be described in terms of the convolution ODA kernel K_{ODA} [12]. Second the wave itself is not anymore deterministic but a random time shift can be observed and described in terms of a Brownian motion B_z. More precisely, the pulse front that can be recorded at the surface is

$$u_s(t,\mathbf{x},z=0) = \frac{1}{(2\pi)^3\varepsilon^2}\int \frac{1}{2\sqrt{I_0(\kappa)}}\,\mathrm{e}^{-\mathrm{i}(\omega/\varepsilon)(t-t_s-\boldsymbol{\kappa}.(\mathbf{x}-\mathbf{x}_s)+\zeta_0(\kappa)z_s)}\hat{K}_{\mathrm{ODA}}(\omega,\boldsymbol{\kappa})S_a(\omega,\boldsymbol{\kappa})\omega^2\,\mathrm{d}\omega\,\mathrm{d}\boldsymbol{\kappa},$$

where $\hat{K}_{\mathrm{ODA}}(\omega,\boldsymbol{\kappa}) = \exp(\mathrm{i}\sqrt{\gamma(\omega,\kappa)}B_{z_s} + \gamma(\omega,\kappa)z_s/2)$. A stationary phase argument shows that the leading order contribution is associated with the stationary slowness vector $\boldsymbol{\kappa}_s = (\mathbf{x}-\mathbf{x}_s)/\sqrt{z_s^2+|\mathbf{x}-\mathbf{x}_s|^2}$. If we denote the longitudinal velocity in homogeneous medium by u_s^{hom} (see Eq. (24)), then in presence of randomness the longitudinal velocity field can be written as the unperturbed front convoluted with a deterministic Gaussian kernel and randomly shifted

$$\begin{aligned} u_s(t,\mathbf{x},z=0) &= [u_s^{\mathrm{hom}}(\cdot,\vec{\mathbf{r}}=(\mathbf{x},0)) * \mathcal{N}_{\mathbf{x}}]\left(t - \frac{\sqrt{\gamma_{\mathbf{x}}}}{\sqrt{2}c_0}B_{z_s}\right), \\ \mathcal{N}_{\mathbf{x}}(t) &= \frac{c_0}{\sqrt{\gamma_{\mathbf{x}}|z_s|\pi}}\exp\left(-\frac{c_0^2t^2}{\gamma_{\mathbf{x}}|z_s|}\right),\ \gamma_{\mathbf{x}} = \gamma_0\frac{\sqrt{|\mathbf{x}-\mathbf{x}_s|^2+z_s^2}}{|z_s|}. \end{aligned} \tag{A.7}$$

References

[1] M. Asch, W. Kohler, G. Papanicolaou, M. Postel, B. White, Frequency content of randomly scattered signals, SIAM Rev. 33 (1991) 519–625.

[2] G. Bal, G. Papanicolaou, L. Ryzhik, Self-averaging in time reversal for the parabolic wave equation, Stochast. Dyn. 2 (2002) 507–531.

[3] P. Blomgren, G. Papanicolaou, H. Zhao, Super-resolution in time-reversal acoustics, J. Acoust. Soc. Am. 111 (2002) 230–248.

[4] R. Burridge, G. Papanicolaou, B. White, Statistics for pulse reflection from a randomly layered medium, SIAM J. Appl. Math. 47 (1987) 146–168.

[5] V. Casulli, R. Cheng, Semi-implicit finite difference methods for three-dimensional shallow water flow, Int. J. Numer. Meth. Fluids 15 (1992) 629–648.

[6] J. Chillan, J.-P. Fouque, Pressure fields generated by acoustical pulses propagating in randomly layered media, SIAM J. Appl. Math. 58 (1998) 1532–1546.

[7] J.-F. Clouet, J.-P. Fouque, Spreading of a pulse traveling in random media, Ann. Appl. Probab. 4 (1994) 1083–1097.

[8] J.-F. Clouet, J.-P. Fouque, A time-reversal method for an acoustical pulse propagating in randomly layered media, Wave Motion 25 (1997) 361–368.

[9] A. Derode, A. Tourin, J. de Rosny, M. Tanter, S. Yon, M. Fink, Taking advantage of multiple scattering to communicate with time reversal antennas, Phys. Rev. Lett. 90 (2003) 014301.
[10] M. Fink, Time reversed acoustics, Sci. Am. (1999) 91–97.
[11] M. Fink, G. Montaldo, M. Tanter, Time reversal acoustics in biomedical engineering, Annu. Rev. Biomed. Eng. 5 (2003) 465–497.
[12] J.-P. Fouque, K. Sølna, Time-reversal aperture enhancement, SIAM Multiscale Model. Simulat. 1 (2003) 239–259.
[13] W.A. Kuperman, W.S. Hodgkiss, H.C. Song, T. Akal, C. Ferla, D.R. Jackson, Phase conjugation in the ocean, experimental demonstration of an acoustic time-reversal mirror, J. Acoust. Soc. Am. 103 (1998) 25–40.
[14] P. Lewicki, R. Burridge, G. Papanicolaou, Pulse stabilization in a strongly heterogeneous medium, Wave Motion 20 (1994) 177–195.
[15] L. Mandel, E. Wolf, Optical Coherence and Quantum Optics, Cambridge University Press, Cambridge, 1995.
[16] G. Papanicolaou, L. Ryzhik, K. Sølna, Statistical stability in time reversal, SIAM J. Appl. Math. 64 (2004) 1133–1155.
[17] C. Pires, M.A. Miranda, Tsunami waveform inversion by adjoint methods, J. Geophys. Res. 106 (2001) 19733–19796.
[18] C. Prada, E. Kerbrat, D. Cassereau, M. Fink, Time reversal techniques in ultrasonic nondestructive testing of scattering media, Inverse Problems 18 (2002) 1761–1773.
[19] R. Snieder, Imaging and averaging in complex media, in: J.-P. Fouque (Ed.), Diffusive Wave in Complex media, NATO Science Series C, vol. 531, Kluwer, 1999, pp. 405–454.
[20] K. Sølna, Focusing of time-reversed reflections, Wave. Random Media 12 (2002) 365–385.
[21] G.B. Whitham, Linear and Nonlinear Waves, Wiley, New York, 1974.